A Thesis

On

Preparation of modified ZnO nanoparticles by sol-gel process and their characterization

Submitted in the partial fulfillment of requirement for the degree of

Master of Technology

in

Material Science and Engineering

by

Ranvir Singh Panwar

(60702017)

Under the supervision of

Dr. K.K. Raina

(Prof. & Deputy Director)

Thapar university, Patiala (Punjab)

School of Physics and Materials science

Thapar University, Patiala, (Punjab)

June-2009

CERTIFICATE

I hereby certify that the work which is being presented in the thesis entitled, **"Preparation of modified ZnO nanoparticles by sol - gel process and their characterization"** in partial fulfillment of the requirements for the award of degree of Master of Technology in **Material Science and Engineering** submitted in School of Physics and Materials Science of Thapar University, Patiala, is an authentic record of my own work carried out under the supervision of **Prof. K. K. Raina** and refers other researcher's works which are duly listed in the reference section.

This is to certify that the above statement made by the candidate is correct and true to the best of my knowledge.

(Prof. K.K. Raina)
Deputy Director,
Dean of Faculty affairs, Dean of RPG
Thapar University, Patiala Punjab. -147004

Countersigned by:

Dr. O.P. Pandey
Prof. and Head,
Thapar University,
Patiala, Punjab.

Dr. R.K. Sharma
Dean, Academic Affairs
Thapar University,
Patiala, Punjab.

Acknowledgment

I am submitting my thesis report and this work would not have been accomplished without the support, help and guidance of a large number of people. I express my deep gratitude and respect to my supervisor **Dr. K.K. Raina, Professor and Deputy Director, School of Physics and Material Science**, for his keen interest, strong motivation and constant encouragement during the course of the work. I thank him for his great patience, constructive criticism and myriad useful suggestions apart from invaluable guidance to me.

I am grateful to **Dr. O.P. Pandey, Professor and Head, School of Physics and Materials Science** for his encouragement and execution of thesis work.

I would also like to thank **Dr. Kulvir Singh, Assistant Professor and PG Incharge, School of Physics and Materials Science** for his constant guidance and encouragement. I am also thankful to **Dr. D.P. Singh, Dr. S.D. Tiwari** and all the faculty members of School of Physics and Materials Sciences for their constructive suggestions at different stages of this work.

It gives me immense pleasure to express my special thanks to **Mr. Ravi Shukla** (Ph.D. scholar), who always took keen interest in guiding me during my work.

I am extremely thankful to **Mr. Deepak Teotia, Mr. Nitin and Mr. Mukesh Kumar** in IIT Roorkee, without whom the work would not have been possible.

I would like to convey my sincere gratitude to my friends and colleagues **Dr. Pankaj Kumar, Ms. Shikha kapila, Ms. Neeraj Sharma, Akash Katoch, Preeti Makkar, Dushyant Tomer, Shivani, Umesh, Pradeep Teotia and Kamal Sangar** for their support and their timely help and valuable discussions.

I owe my sincere thanks to all the staff members of School of Physics and Materials Science for their support and encouragement.

Last but not the least; I would like to thank to my wife **Mrs. Shalu Panwar** for her patience, moral support and constant co-operation whenever I was away from her.

The meaning of my life and work is incomplete without paying regards to my respected parents whose blessings and continuous encouragement have shown me the path to achieve my goals. And above all, I pay my regards to the **Almighty** for his love and blessings.

Ranwar.

(Ranvir Singh Panwar)

Abstract

A novel sol gel method was utilised to synthesis ZnO powder as pure and in the presence of different surfactants CTAB (N–Cetyl–N,N,N,trimethyl ammonium bromide), CPCl (Cetyl pyridinium chloride) and Silica gel in basic medium by adjusting the pH around 9. ZnO powder were prepared from hydrated Zinc acetate precursor ($(C_2H_3O_2)_2Zn.2H_2O$) and ethyl alcohol solvent. The synthesized powder was calcined at 400^0 C for 1 hour. Structural, morphological, thermal and chemical properties of synthesized ZnO powder were investigated by X-ray diffraction (XRD), scanning electron microscopy (SEM), thermo gravimetric analysis (TGA) and Fourier transform infra red microscopy (FTIR) respectively. Our finding shows the formation of pure phase of ZnO in basic medium in presence of different surfactants. The calculated particle size of ZnO powder was in the range of 3 to 15 nm. In addition we also made an attempt to dope the Di and Ag on ZnO. Structural characterization shows the formation of pure phase of ZnO up to 1% Di. However at higher concentration (3%and 5%) we found mixed phase. On the other hand in case of Ag doping the system has mixed phase which indicates that Ag remains unreacted in the reaction.

CONTENTS

List of Figures

List of Tables

Chapter 1

Introduction

Introduction

1.1 Brief overview of ZnO characteristics:

The unique and fascinating properties of II-VI compound semiconductors have triggered tremendous motivation among the scientists to explore the possibilities of using them in industrial applications, Zinc oxide (ZnO) is a piezoelectric, dielectric, transparent, semiconducting oxide, with a direct band gap of 3.37 eV at room temperature and a large excitation binding energy (60 meV), which is 2.4 times the effective thermal energy (K_{BT} =25meV) at room temperature, and biexcitation energy is 15meV. This is one of the key parameters that ZnO exhibits near-UV emission, transparency, conductivity, and resistance to high temperature electronic degradation. In addition, ZnO is the hardest of the II-VI semiconductors due to the higher melting point (2248k) and large cohesive energy (1.89ev) (therefore more resistant to wear), as well as one of the most piezoelectric semiconductors (d= 12.2×10^{-12} C/N) with good piezoelectric coefficient K_L =0.27 and its high adherence on various substrates[1-4].

There are also possible applications in micro electromechanical systems (MEMS), both in sensors, actuators and in the fabrication of acoustic and electro-optical devices. In particular, it can be used as bulk acoustic wave (BAW) resonators and as thin film bulk acoustic wave (FBAR) resonators or surface acoustic wave (SAW) resonators [4]. It is commonly used as a catalyst, piezoelectric transducer, and photonic material. ZnO has several fundamental advantages over its chief competitor GaN and SiC. In fact, its free exciton is bound with 60 meV, much higher than that of GaN (21–25 meV); high energy radiation stability and amenability to wet chemical etching (although both are much better than Si or GaAs). Furthermore several experiments verified that ZnO is very resistive to high energy radiation, making it suitable candidate for space applications. It can be easily etched in all acids and alkalis. Due to this reason it can be used in the fabrication of small size devices e.g. transparent electrodes, window materials for displays and solar cells. It has also native substrate [2]. Moreover it is used in a variety of technical applications, including porcelain enamels, heat resisting glass, an activator in vulcanization, an additive for rubber and plastics, pigment in paints with UV-protective and fungistatic properties, spacecraft protective coatings, a constituent of cigarette filters, healing ointments, in optical waveguide, and many more [5]. ZnO has played an important role in the fabrication of transparent thin film

transistors (TFT), by depositing channel layer on a flexible substrate through low temperature processes, realizing transparent TFTs, and achieving extra functions such as photodetections using ZnO channel. In this case the protective covering to prevent light exposure is eliminated since ZnO based transistors are insensitive to visible light. The deposited ZnO usually maintains a crystalline phase, although the deposition process is carried out even at room temperature [6, 7].

The films of Zinc oxide (ZnO), indium tin oxide (ITO), and cadmium oxide (CdO) have been investigated in recent years as transparent conducting oxide (TCO) due to their good electrical and optical properties in combination with large band gap(>3ev), abundance in nature, optical transmittance (>80%) in visible region and absence of toxicity [8]. Besides, this zinc oxide has received particular attention as a promising substrate material due to it isomorphic structure. Low conductivity ZnO single crystal substrates have numerous advantages for both nitride and oxide based devices in base station wireless power amplifier applications. Low substrate defect density coupled with the isomorphic wurtzitic lattice with respect to GaN result in films that reward device manufacturers with better performance. The semi-insulating property of the substrate prevents parasitic currents in field effect transistors as well as permitting direct electrical characterization of epitaxial films especially in thin film form, since bulk ZnO is quite expensive and unavailable in large wafers for the time being, interfacial energy between ZnO and sapphire or other oxide substrate is such like that it always favoured two- dimensional growth, which results in high quality film at lower temperatures (less than 700ºC) [9]. ZnO is a promising material for spintronics applications because of theoretical predictions of room temperature ferromagnetism, for example Curie temperature of > 300K for Mn-doped p-type ZnO and n-type doping in Fe-, Co-, or Ni-alloyed. ZnO have gained intense attention in the searching for high temperature dc Curie (Tc) ferromagnetic diluted magnetic semiconductors (DMS) materials, which are based on ZnO. DMSs could exhibit ferromagnetism above room temperature upon doping with transition elements [2, 8].

ZnO crystallizes in two different crystal lattices. The first is the hexagonal wurtzite lattice which is mainly used in thin film industry as a transparent conducting oxide (TCO) or as a catalyst in methanol synthesis. The second structure is more known to geologist as the rock salt structure (at high pressure) and is a spinal phase that is used in the understanding of the earth's lower mantle. But a thermodynamically stable phase is the wurtize structure, which is well known to show piezoelectric properties with a large electromechanically coupling factor and a low dielectric constant $\varepsilon(0) = 8.75$ to $\varepsilon(\infty) = 3.75$.

1.2 Comparison of different semiconductors:

ZnO was one of the first semiconductors to be prepared in rather pure form after silicon and germanium. It was extensively characterized as early as the 1950's and 1960's due to its promising piezoelectric/acoustoelectric properties. Wide band gap semiconductors have gained much attention during last decade because of their possible uses as optoelectronic devices in the short wavelength and ultraviolet (UV) portion of the electromagnetic spectrum. These semiconductors such as ZnSe, ZnS, GaN, and ZnO, have shown similar properties with their crystal structures and band gaps. As shown in table 1.1, some of the important properties of these wide band gap semiconductors are summarized. Initially, ZnSe based devices and the GaN based technologies obtained large improvements such as blue and UV light emitting diode and injection laser. ZnSe has produced some defect levels under high current drive. No doubt, GaN are considered to be the best candidate for the optoelectronic devices. However, ZnO has great advantages for light emitting diodes (LEDs) and laser diodes (LDs) over the currently used semiconductors. Recently, it has been introduced that ZnO as II–VI semiconductor is promising for various technological applications, especially for optoelectronic short wavelength light emitting devices due to its wide and direct band gap. The most important advantage is the high exciton binding energy (60 meV) giving rise to efficient exitonic emission at room temperature. Since ZnO and GaN have almost identical lattice parameters and the same hexagonal wurtzite structure, ZnO can satisfactorily be used as lattice matched substrate in GaN based devices or vice versa. ZnO has excellent radiation hardness among all other semiconductors. This property supplies the uses of ZnO based devices in space applications and high energy radiation environments. Band gap energy can be varied from 3.3 eV up to 4.5 eV with alloying process. Hence it can be used as an active layer in the doubly confined hetero-structured LEDs and quantum well lasers. These unique nanostructures unambiguously demonstrate that ZnO is probably the richest family of nanostructures among all materials, both in structure and properties [2, 10, 23].

Table 1.1: Comparison of different semiconductors

Wide band gap semiconductor	Crystal structure	Lattice parameter (A^o)		E_g (eV at RT)	Melting temp. (K)	Excitation binding energy (MeV)	Dielectric constant	
		a	b				ε_o	ε_∞
ZnO	Wurtzite	3.250	5.206	3.37	2248	60	8.75	3.72
GaN	Wurtzite	31.89	51.85	3.4	1973	21	9.5	5.15
ZnSe	Zinc-blende	5.667	-	2.7	1790	20	7.1	5.3
ZnS	Wurtzite	3.824	6.261	3.7	2103	36	9.6	5.7

1.3 Fundamental properties of ZnO

1.3.1 Crystal structure

Zinc oxide crystallizes in three forms: hexagonal wurtzite, cubic zinc blende, and the rarely observed cubic rocksalt). The wurtzite structure is most stable and thus most common at ambient conditions. The zincblende form can be stabilized by growing ZnO on substrates with cubic lattice structure. In both cases, the zinc and oxide are tetrahedral. The rocksalt NaCl-type structure is only observed at relatively high pressures - ~10 GPa. The hexagonal and zincblende ZnO lattices have no inversion symmetry (reflection of a crystal relatively any given point does not transform it into itself). This and other lattice symmetry properties result in piezoelectricity of the hexagonal and zincblende ZnO, and in pyroelectricity of hexagonal ZnO. The lattice constants are a = 3.25 Å and c = 5.2 Å; their ratio c/a ~ 1.60 is close to the ideal value for hexagonal cell c/a = 1.633. As in most II-VI materials, the bonding in ZnO is largely ionic , which explains its strong piezoelectricity . Due to this ionicity, zinc and oxygen planes bear electric charge (positive and negative, respectively). Therefore, to maintain electrical neutrality, those planes reconstruct at atomic level in most relative materials, but not in ZnO - its surfaces are atomically flat, stable and exhibit no reconstruction. This anomaly of ZnO is not fully explained yet.

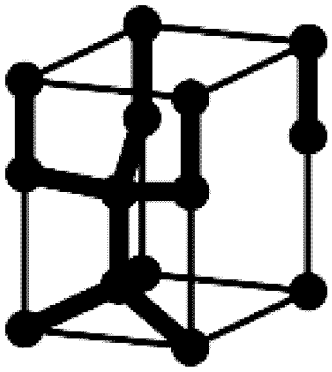

Figure 1.1: Schematic representation of a wurtzitic ZnO structure.

The tetrahedrally coordinated diamond, zinc blende, and wurtzite-type crystal structures have the quality for covalent chemical binding with sp^3 diamond, silicon and germanium have completely covalent bonding, one has an increasing admixture of ionic binding when going from the Group IV over the III–V and II–VII to the I–VII semiconductors, ending with completely ionic binding for the II–VI and I–VII insulators like MgO or NaCl, which frequently crystalline in the rock salt structure.

1.3.2 Lattice parameters

Lattice parameters are considered important, when one has to develop semiconductors devices. There are mainly four factors which determine the lattice parameters of the semiconductors. (i) Free-electron concentration which affects the potential of the bottom of conduction band normally occupied by electrons. (ii) Concentration of impurities and defects and the difference in ionic radii between these defects and impurities with respect to substituted matrix ions. (iii) External strains (for example, those induced by substrate) (iv) temperature. On the other hand, the strict periodicity of the lattice is disturbed by many imperfections or defects. These imperfections or defects have a considerable, controlling influence on mechanical, thermal, electrical and optical properties of semiconductors. They determine the plasticity, hardness, thermal and electrical conductivities. Commonly the lattice parameters of any crystalline material are measured accurately by high-resolution x-ray diffraction (HRXRD). Table 1.2 shows a comparison of measured and calculated lattice parameters of ZnO, c/a ratio reported by several groups [2, 8].

Table 1.2: Measured and calculated lattice constants

	a(A^o)	c(A^o)	c/a
(a)	3.2496	5.2042	1.6018
(b)	3.2501	5.2071	1.6021
(c)	3.286	5.241	1.595

[a] Measured by using x-ray diffraction.

[b] Measured by using powder x-ray diffraction.

[c] Calculated by using ab-initio periodic linear combination of atomic orbital (LCAO) method

1.3.3 Electronic band structure

A very important property of any given semiconductor is its band structure, because many important properties such as the band gap and effective electron and hole masses are derived from it. ZnO is considered most suitable semiconductor among all his family members for ultraviolet lasing at room temperature, device application as well as possibilities to engineer the band gap, for this reason a clear understanding of the band structure is important to explain the electrical properties and many other phenomena because it determines the relationship between the energy and the momentum of the carrier.

Experimental methods to determine band structure normally involve measurements by UV and X-ray reflection/absorption/ emission techniques as well as photoelectron spectroscopy (PES) and angular resolved photoelectron spectroscopy (ARPES) has been used to measure the electronic core levels in solids. These methods basically measure the energy difference by inducing transitions between different electronic levels (for example, transitions from the upper valence-band states to the upper conduction states, and the lower valence-band states) [2, 8, 12].

Angular resolved photoelectron spectroscopy (ARPES) along with synchrotron radiation excitation has been recognized as a powerful tool that enables experimental bulk and surface electronic band-structure determination under the assumption of k conservation and single nearly free electron like final band. The other important method for the analysis of the energy region is based on photoelectric effect extended to X-ray region, namely, photoelectron spectroscopy (PES). The peaks in emission spectrum correspond to electron emission from a

core level without inelastic scattering, which is usually accompanied by a far-less-intense tail region in the spectrum.

The most important aspect of the band structure of ZnO is that it has a direct band gap. Recently the band structure was calculated using an empirical tight –binding Hamiltonian. Band gap between the occupied band and empty bands optical band gap (E_g) of ZnO is about 3.3eV. Actually this is the energy difference between full and empty state.

These filled states are called the *valence band*, and the energy at the top of the valence band is usually *zero energy* and is called *valence band edge*. The empty states above the gap are called the *conduction band*. The lowest point in the conduction band is called the *conduction band edge*. Since for ZnO the valence band and the conduction band edges occur at the same k-values, the material is called a *direct band gap semiconductor* [13, 14].

1.3.3.1 Band gap engineering

In order to make progress in modern devices, like ZnO UV detector and field effect transistors (FET), modulation of the band gap is required. It has been verified due to the development of $Mg_xZn_{1-x}O$ and $Be_zZn_{1-z}O$ alloys for larger band gap material and $Cd_yZn_{1-z}O$ alloy for smaller band gap material, allowing band gap tuning in a wide range. The energy gap Eg(x) of a ternary semiconductor $A_xZn_{1-x}O$ (where A =Mg, Be, and Cd) is determined by the following empirical equation.

$$\mathbf{Eg(x)= (1-x)E_{ZnO} + xE_{AO} – bx(1-x)} \qquad \mathbf{2.2}$$

Where b is the bowing parameter and E_{AO} and E_{ZnO} are the band gap energies of compounds AO (MgO, CdO, BeO) and ZnO, respectively. The bowing parameter depends on the difference in the electronegativities of the end binaries ZnO and AO. The band gap vs. the in-plane lattice is constant for all ternaries, namely $Be_zZn_{1-z}O$, $Mg_xZn_{1-x}O$ and $Cd_yZn_{1-z}O$ is shown in fig. 1.2. $Mg_xZn_{1-x}O$ alloys are considered as a suitable material for barrier layers in ZnO/ (Mg, Zn) O superlattice structures. Because alloying ZnO with MgO (Eg ~ 7.7 eV) enables widen the band gap of ZnO with very little change in the lattice constant.

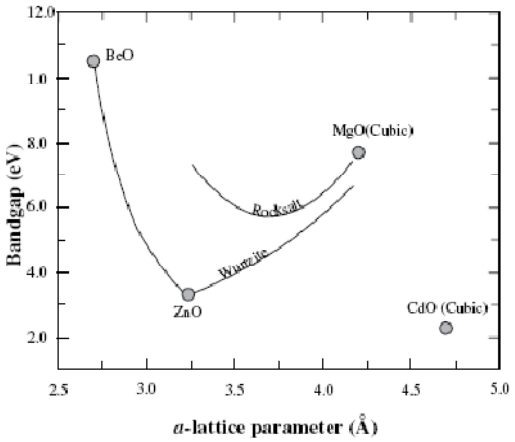

Figure 1. 2: Band gap vs. in-plane lattice constant for the ternaries of ZnO, namely, $Be_zZn_{1-z}O$, $Mg_xZn_{1-x}O$, and $Cd_yZn_{1-y}O$.

ZnO has a wurtzite structure (a = 3.24 Å and c = 5.20 Å), while MgO has a cubic structure (a = 4.24 Å). $Mg_xZn_{1-x}O$ with composition up to near 40% and band gap near 4 eV remains wurtzitic, but after the composition of near about 60% their structures become cubic. In the intermediate region the quality of the film is not good due to conversion of different mixed polytypes are present in it. Substitution of Be for Zn increases the band gap of ZnO. Unlike MgZnO, which changes over to the cubic form beyond the 40% Mg concentration, $Be_zZn_{1-z}O$ is wurtzitic throughout the entire compositional range as the equilibrium state of BeO is wurtzitic. For narrower band gaps, which are desirable for wavelength tunability and attaining band gaps corresponding to the visible spectrum, $Cd_yZn_{1-z}O$ alloy would be a good candidate because of the small direct band gap of CdO (2.3 eV). There has not been as much progress with Cd doped ZnO. We should mention that CdO is cubic also and large concentrations of Cd in ZnO lattice would cause a behavior similar to the MgZnO case in the intermediate region [15, 16].

1.3.4 Properties of wurtzite ZnO

Table 1.3 shows a compilation of the basic physical parameter for ZnO. Still some uncertainty exists in these values. For example, in few reports it has been mentioned physical properties of only p-type ZnO and therefore the hole mobility and effective mass are still in debates [10, 11].

Table 1.3: Basic physical properties of ZnO

Property	value
Lattice parameter at 300 K	
a	3.2495 A^o
c	5.2069 A^o
c/a	1.602
Density	5.606 g cm^{-3}
Stable phase at 300 K	Wurtzite
Bond length	1.977 μm
Melting point	1975^oC
Thermal conductivity	0.6 , 1-1.2
Static dielectric constant	8.656
Refractive index	2.008, 2.029
Energy gap	3.4 eV, direct
Exciton binding energy	60 MeV
Iconicity	62%
Heat capacity Cp	9.6cal/mol K
Youngs modulus E(Bulk ZnO)	111.2±4.7 Gpa

1.3.4.1 Optical Properties

The optical properties of a semiconductor are associated with both intrinsic and extrinsic effects. Intrinsic optical transitions take place between the electrons in the conduction band and holes in the valence band, including excitonic effects due to the Coulomb interaction. The main condition for exciton formation is that the group velocity of the electron and hole is equal. Excitons are classified into free and bound excitons. In high quality samples with low impurity concentrations, the free exciton can also exhibit excited states, in addition to their ground-state transitions. Extrinsic properties are related to dopants or defects, which usually create discrete electronic states in the band gap, and therefore influence both optical-absorption and emission processes. As we mentioned above, that ZnO is a direct band semiconductor and a transparent conductive material. ZnO films are transparent in the wavelength range of 0.3 and 2.5 μm, and plasma edge lies between 2 and 4 μm depending on the carrier concentration. It is well known that a shift in the band gap edge appears with an increase in the carrier concentration. This shift is known as Burstein-Moss shift. Optical transitions in ZnO have been studied by a variety of experimental techniques such as optical absorption, transmission, reflection, spectroscopic. ellipsometry, photoluminescence, cathodoluminescence, calorimetric spectroscopy, etc. Room temperature PL spectrum of ZnO

is usually composed of a near UV-emission band (375 nm) and a green emission band (510 nm) although a yellow-orange band (610 nm) can also be observed in some situations. The near UV-band is closely related to the excitonic nature of the material and may be superposed with the free exciton emission, its phonon replica, bound exciton emission, as well as biexciton emission. The observation of luminescence from exciton is usually difficult even at low temperatures. This comes from a lot of factors [17]: First, the efficiency of radiative emission is low even for direct gap semiconductors, which is often found to be 10^{-1} to 10^{-3}. A large part of the radiative emission comes from bound-exciton complexes and defect centers. Second, exciton emission is limited by the internal reflection of the exciton and the small escape length. As a quasi-particle, exciton moves with their group velocity through the semiconductor. During its movement, exciton can be trapped or scattered by impurities and phonons. When it eventually reaches the surface of the semiconductor, in most cases, it will be reflected back into the semiconductor. Except the internal reflection, the radiative combination yield from free-exciton is also limited by the small escape length, which is defined as the depth from which exciton can reach the surface. Only the free-exciton inside the escape length can have the contribution to the luminescence. The research interest for the green band emission in ZnO can be traced back to the early stage of last century. Due to this green emission, ZnO is considered as an important luminescent material for the planar display and short-decay cathodoluminescence screens. Unfortunately, the mechanisms behind this emission band are still unclear even though the researches on this topic have been lasted for many years. Green band emission was first attributed to an excess of zinc. Almost all the proposed mechanisms about the green emission are attributed to the native lattice defects except the one that is based on the divalent Cu impurities.

1.3.4.2 Thermal Properties

Thermal expansion coefficient (TEC)

The change in temperature affects the lattice parameters of semiconductors. Thermal expansion coefficient, are defined as — or α_a and — or α_c for in and out of plane cases, respectively. The stichiometry, presence of extended defects and free carrier concentration also affect the thermal expansion coefficient. The X-ray powder diffraction method by Reeber was used to measure the temperature dependence of lattice parameters of ZnO as shown in Figure 1.3. Lattice parameters of ZnO were measured over the temperature range 4.2 -299 K, fourth-order polynomials were fitted using the least-squares method, which gives

the minimum for the a_0 parameter at 93 K. The c_0 parameter has much uncertainty, did not give any minimum value, perhaps due to its less precision and uncertainty in measurement [19].

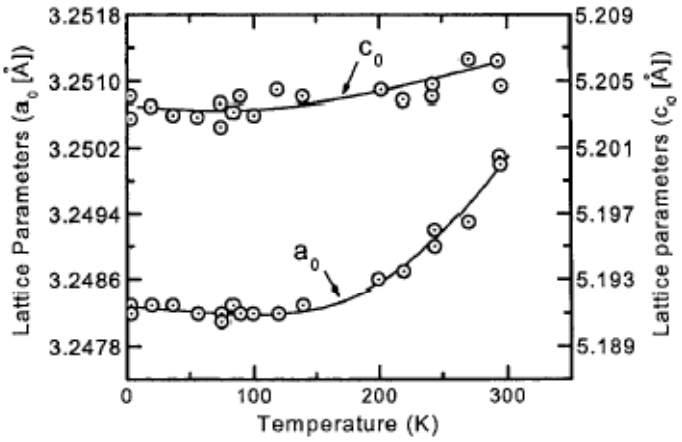

Figure 1.3: Wurtzite ZnO lattice parameters as a function of temperature.

Thermal conductivity

Thermal conductivity (k), having a kinetic nature, is determined by vibration, rotation and electronic degree of freedom. It is really important property of semiconductors when these materials are used in high-power, high-temperature or optoelectronic devices. The electronic thermal conductivity is very small, having light carrier concentration, which is negligible. For high pure crystals, phonon-phonon scattering is ideally proportional toT^{-1} at the temperatures higher than the Debye temperature. Point defects, such as vacancies, impurities and isotope fluctuations in a ZnO affect the thermal conductivity of ZnO material.

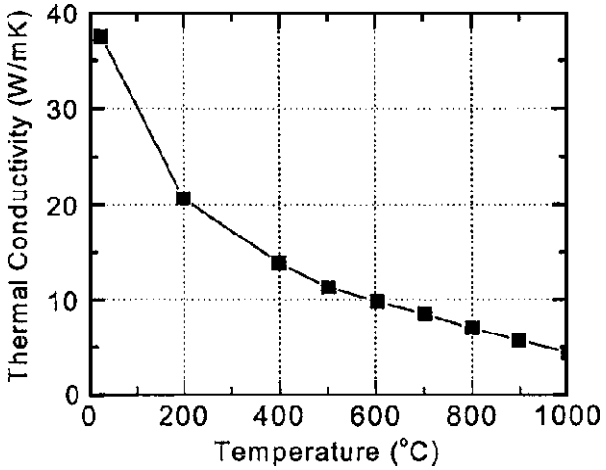

Figure 1.4: Thermal conductivity of fully sintered ZnO heated from room temperature to 1000 °C

The thermal conductivity of fully sintered ZnO at temperatures from room temperature to 1000°C is measured. Fig.1.4 shows the thermal conductivity curve for a fully dense ZnO crystal. The thermal conductivity decreases from 37 to 4 W/m K as the temperature is increased from room temperature to 1000 °C. The dominant scattering mechanism is resistive phonon-phonon interactions (umklapp process) [20].

1.3.4.3 Electrical Properties

As a direct and wide band gap semiconductor with a large exciton binding energy (60meV), ZnO is representing a lot of attraction for optoelectronic and electronic devices. For example, a device made by material with a larger band gap may have a high breakdown voltage, lower noise generation, and can operate at higher temperatures with high power operation. The performance of electron transport in semiconductor is different at low and high electric field. At sufficient by low electric fields, the energy distribution of electrons in ZnO is unaffected much, because the electrons can't get much energy from the applied electrical field, as compared with their thermal energy. So the electron mobility will be constant because the scattering rate, which determines the electron mobility, doesn't change much When the electrical field is increased, the energy of the electrons from the applied electrical field is equivalent to the thermal energy of the electron. The electron distribution function changes significantly from its equilibrium value. These electrons become hot electrons, whose temperature is higher than the lattice temperature. So there is no energy loss to the lattice during a short and critical time. When the electron drift velocity is higher than its steady-state value, it is possible to make a higher frequency device

1.4: Doping and defects in ZnO

In the recent years, much attention has been focused on wide band gap semiconductors materials because of their excellent potential for blue light emitting devices, short-wavelength laser diodes and detectors in UV-blue spectral region. As wide band gap ZnO is gaining much importance for the possible application due to the capability of ultraviolet lasing at room temperature and possibilities to engineer the band gap. In order to attain the potential offered by ZnO, both high-quality n-and p-type ZnO are essential. But it is very difficult to obtain the bipolar carrier doping (both n and p types) in wide-band-gap semiconductors such as GaN and II-VI compound semiconductors including ZnS, ZnSe, and ZnTe .Unipolar

doping has not been a surprising issue in wide-band-gap semiconductors: ZnO, GaN, ZnS, and ZnSe are easily doped to n-type , while p-type doping is difficult. All undoped ZnO to date has been found to be n-type, with donor concentrations typically around 10^{17} cm^{-3} for present-day, high-quality material, but sometimes as high doped material. The situation is opposite for ZnTe where p-type doping is easily obtained, while n-type doping is difficult. The main characterization techniques used to find the shallow electrical defects in semiconductor materials are photoluminescence and temperature dependent Hall Effect measurements.

N-type doping

ZnO has wurtzite structure, excess zinc is always found in ZnO. Due to this zinc excess, ZnO is a non-stoichiometric compound and n-type semiconductor. Undoped ZnO shows intrinsic n-type conductivity with high electron densities of about 10^{21} cm^{-3}. Zinc interstitials Z_{ni} and the oxygen vacancy V are known the dominant native donor in unintentionally ZnO film. But still it is debatable issue. Photoluminescence and temperature dependent Hall studies of electron irradiated ZnO have shown that zinc is the most likely candidate for purely lattice-related dominant shallow donor, with an activation energy about 30-50 meV. It has been argued that the n-type conductivity of unintentionally doped ZnO film is only due to hydrogen (H), which is treated as a shallow donor with activation energy of 31 meV instead of Zni. This assumption is valid because hydrogen (H) is always present in all growth methods and can easily diffuse into ZnO in large amounts due to it large mobility [22]. Hydrogen has been considered as a shallow donor candidate, much research has been done on hydrogen (H) in ZnO. During seeded chemical vapor transport (SCVT) growth of ZnO, it has been shown that hydrogen with activation energy 39 meV acts as main donor. This donor disappears through on annealing process. [12, 22].

N-type doping of ZnO is relatively easy as compared to p-type doping. Group III elements Al, Ga and In as substitutional elements for Zn and group-VII elements Cl and I as substitutional elements for O can be used as n-type dopants. Doping with Al, Ga, and In has been attempted by many groups, resulting in high-quality, highly conductive n- type ZnO films. Al-doped ZnO films were grown by MOCVD. The films obtained through this method is high by conductive with minimum resistivity as compared to Ga- doped ZnO films be Chemical-vapor deposition [2, 12].

P-type doping

It is very difficult to obtain p-type doping in wide band gap semiconductors. Acceptors in ZnO can also take place from both lattice defects and impurity atoms. The oxygen interstitial O_i and zinc vacancy V_{zn} are both known to be acceptors in ZnO. P-type doping in ZnO may be possible by substituting either group-I elements (Li, Na, and K) for Zn sites acting as shallow acceptors and group-V elements (N, P, and As) are found to act as deep acceptors on O sites. It was shown that group-I elements could be better p-type dopants than group-V elements in terms of shallowness of acceptor levels. However, group-I elements tend to occupy the interstitial sites, due to their small atomic radii, rather than substitutional sites, and therefore, they act as donors instead of acceptors. Moreover, significantly larger bond length for Na and K than ideal Zn–O bond length (1.93 Å) induces lattice strain, increasingly forming native defects such as vacancies which compensate the shallow dopants. Group V elements (N, P, As) except N, both P and As, have a larger bonds lengths. That's why they are likely to form antisites to avoid the lattice strain. Unfortunately for p-conduction these elements have a tendency towards antisite formation, i.e. they can substitute not only oxygen but also zinc atoms, in which case they act as donors. Nitrogen (N) appears to be good candidate for a shallow P-type dopant in ZnO with smallest ionization energy, although N is not soluble in ZnO, and doping can be achieved by ion implantation [2, 12, 25,].

1.5 Aim of work:

Functional materials have been found to exhibit interesting properties like electronic, semi-conducting, piezoelectricity etc. Among these metal oxides family, particularly Zinc oxide has become a material of interest among scientific community, due to the commercial importance as additive in paints and protective coating of metals. The main objective of the study is to obtained the different morphology in presence of different surfactants like N–Cetyl – N,N,N,Trimethyl ammonium bromide (CTAB), Cetyl pyridinium chloride (CPCl) and silica gel in basic medium. Further we will dope rare earth metal to get enhanced properties of ZnO.

The main objectives are:

- Synthesis of ZnO in basic medium and its characterization.
- To grow ZnO in the presence of different surfactants CTAB, CPCl and Silica gel.
- To study the effect of Di and Ag doping on ZnO

1.6. LITERATURE REVIEW

Zinc oxide (ZnO) is no stranger to scientific study. In the past 100 years, it has featured as subject of thousands of research papers, dating back as early as 1935 [26]. Valued for its ultra violet absorbance, wide chemistry, piezoelectricity and luminescence at high temperatures, ZnO has penetrated far into industry, and is one of the critical building blocks in todays modern society [27]. It can be found in paints, cosmetics, plastic and rubber manufacturing, electronics and pharmaceuticals, to name just a few. More recently however, ZnO has again entered the scientific spotlight, this time for its semiconducting properties [28]. Fueled out of advances in growth technologies and the potential for ZnO to become a suitable substrate for GaN, the fabrication of high quality single crystals and epitaxial layers was achieved [29, 30]. Allowing for the realisation of ZnO-based photonic and optoelectronic devices, where, amongst other potential applications it stands with GaN as a prospective candidate for the next generation of light emitters for solid state lighting applications [30,31]. With a wide band gap of 3.4 eV and a large exciton binding energy of 60 meV at room temperature, ZnO holds excellent promise for blue and ultra-violet optical devices. Although in the past GaN and GaN-based materials have dominated this wavelength range, ZnO enters the arena with several advantages [32, 33]. The two most crucial of these are: 1. The larger exciton binding energy, which will allow for room temperature devices operating with higher efficiency and lower power threshold for lasing by optical pumping. 2. The ability to grow high quality single crystal substrates with relative cost effectiveness and ease - something that still eludes GaN Table 1.1 highlights some of the key properties of ZnO, and provides a comparison with GaN. Other favourable aspects of ZnO include its broad chemistry leading to many opportunities for wet chemical etching, piezoelectric properties, radiation hardness and high ferromagnetic Curie temperature for spintronic applications [34, 35]. Together, these properties make ZnO an ideal candidate for a variety of devices including blue and ultra-violet laser diodes and light emitting diodes [36]. Despite the maturity of the field of semiconductors and the wide information base available for ZnO; as a semiconductor, little is actually known about this material. As with all wide band-gap semiconductors, ZnO has presented a number of hurdles to the scientific community which need to be understood and overcome before ZnO based devices can be commercially realised. Zinc oxide (ZnO) is of great interest as a suitable material for high temperature, high power electronic devices either as the active material or as a suitable substrate for epitaxial growth of group III-nitride

compound UV photoconductivity of ZnO is governed by surface-related and bulk-related processes. The surface-related process is primarily governed by the adsorption and desorption of the chemisorbed oxygen at the surface of the ZnO, which is exploited for gas sensing applications [38]. This process becomes prominent in nanocrystalline films, where the surface area is large. In the bulk-related process, oxygen molecules in the grain boundaries contribute to photoconductivity. The bulk-related process is however considered to be faster in comparison to the surface-related process. For UV-detection, the fast component, due to the generation of photo carriers and their radiative and non-radiative recombination through local centres, is of greater importance [35]. Inherent defect centres, such as oxygen vacancies and zinc interstitials are believed to be responsible for visible photoluminescence in ZnO. Markevich et al. [36] have shown that recombination centers responsible for the orange band were the centers of photosensitivity. Defects in ZnO strongly depend on the preparation and annealing conditions which in turn affect the photoconduction properties. There have been studies on the effect of annealing under different conditions on the defect-related emission of ZnO thinfilms and nanostructures [37-39]. Thus Ghosh et al. [29] find that air-annealed ZnO films are preferable for photodetector applications due to the lower dark current. The large concentration of defects in the ZnO nanostructures prepared at low temperatures can be controlled by annealing in oxygen at different temperatures. It is therefore important to carry out a study of the effect of annealing temperature on the photoluminescence as well as the photoconduction properties of ZnO nanostructures. In this communication, we report the effect of annealing in an oxygen atmosphere on the photoluminescence and photoconducting properties of thin films of colloidal ZnO nanoparticles.

Chapter 2

Methodology and Characterization techniques

Methodology and Characterization techniques

2.1 Materials

The materials used in this study were

- Zinc acetate ($C_2H_3O_2$) $_2Zn.2H_2O$ of M_w =219.5 (s-d fine chemical ltd.)
- Ethanol (C_2H_5OH) of M_w = 46.06 (Merck),
- Sodium hydroxide (NaOH) (M_w= 40.0) (s-d fine chemical ltd),
- CPCl (Cetyl pyridinium chloride) $C_{21}H_{38}ClN.H_2O$ (Loba chemicals),
- CTAB (N–Cetyl–N,N,N,Trimethyl Ammonium Bromide) $C_{19}H_{42}BrN$ (Loba chemicals),
- Silica gel with porosity of 10 A^0 (Aldrich)
- Didymium (mixture of praseodymium and neodymium),
- Dilute Lactic Acid ($CH_3CH(OH)COOH:H_2O$)

2.2 Synthesis of ZnO samples:

The glass wares (three necks round bottom flask, measuring cylinder, beaker) were first cleaned and **rinse** with distilled water and dried in vacuum oven. All the materials and

Figure 2.1 Experimental set up for the sample preparation.

solvents were weighted with help of electronic weighing balance and mixed in cleaned round bottom flask. A 100 ml three neck flask charged with Zinc acetate and ethanol. Different

surfactants, Didymium and silver were doped at different concentration. All the reactions were refluxed at 74^{o}C with gentle stirring for 2-4 h on hot plate shown in figure 2.1. After stirring for 2-4h, reaction mixture allowed to cool **to** room temperature.

Synthesis of ZnO Nanopowder in basic medium:

- **Sample 2- Zno Base:**

Chemical name	**Chemical formula**	**Mole required**	**Material Taken**
Zinc acetate	$(C_2H_3O_2)_2Zn.2H_2O$	0.005	1.1 gm
Sodium hydroxide	NaOH	0.02	0.83 gm
Ethanol	C_2H_5OH	----	100 ml

Whole experiment can be summarized as:

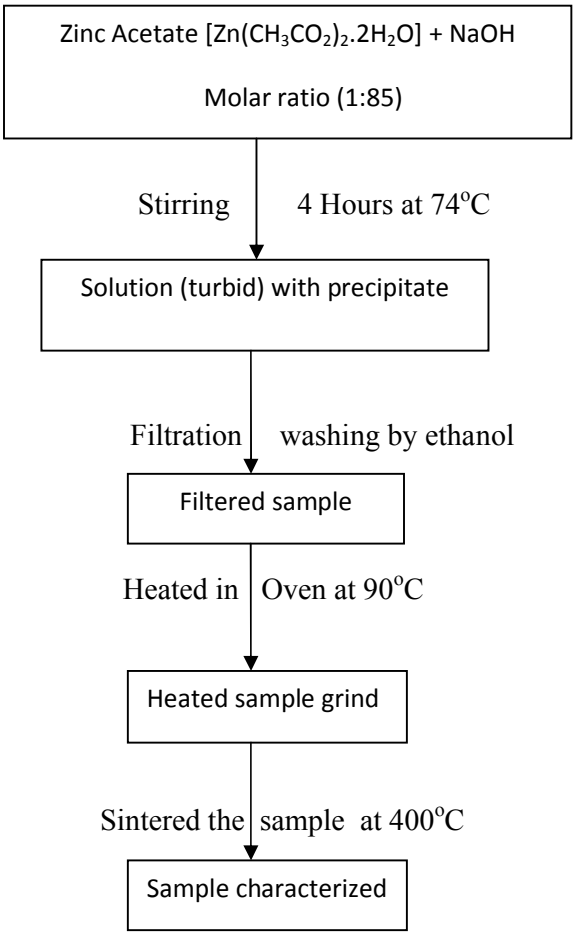

Zno nanopowder was synthesis by sol gel process. Zinc acetate [$Zn(CH_3CO_2)_2.2H_2O$] and NaOH were used as a precursor material and the solvent, respectively. Zinc acetate was

dissolved in NaOH by the molar ratio of 1:85. After stirring the solution with reflux at 70-75^{o} C for 4 hours . Then filtration was done by whatman filter paper. During the filtration solution was washed by ethanol many times to avoid the impurities. After filtration, filtered sample was heated at 90^{o} C in oven for 2 hours. Heated sample was grinded and characterized under many techniques (like XRD, FTIR, SEM, UV etc.)

❖ Synthesis of Zno Nanopowder by using different surfactants:

ZnO nanopowder was also prepared by using different surfactants (like CTAB*,CPCl*) and silica (**Si**) gel were added 0.05% mol. Procedure was same as above. During experiment surfactants were washed out by ethanol.

➢ Sample 3- Zno in presence CTAB:

Chemical name	**Chemical formula**	**Mole required**	**Material Taken**
Zinc acetate	$(C_2H_3O_2)_2Zn.2H_2O$	0.005	1.1 gm
Sodium hydroxide	NaOH	0.02	0.83 gm
Ethanol	C_2H_5OH	---	100 ml
CTAB*	$C_{19}H_{42}BrN$	0.5	0.97 gm

*N– Cetyl – N,N,N,Trimethyl Ammonium Bromide (GR)

➢ Sample 4- Zno in presence of CPCl:

Chemical name	**Chemical formula**	**Mole required**	**Material Taken**
Zinc acetate	$(C_2H_3O_2)_2Zn.2H_2O$	0.005	1.1 gm
Sodium hydroxide	NaOH	0.02	0.83 gm
Ethanol	C_2H_5OH	---	100 ml
CPCl*	$C_{21}H_{38}ClN.H_2O$	0.5	0.97 gm

*Cetyl pyridinium chloride

➢ Sample 5- Zno in presence of Silica gel:

Chemical name	Chemical formula	Mole required	Material Taken
Zinc acetate	$(C_2H_3O_2)_2Zn.2H_2O$	0.005	1.1 gm
Sodium hydroxide	NaOH	0.02	0.83 gm
Ethanol	C_2H_5OH	---	100 ml
Silica gel	SiO_2	0.01	0.60 gm

*CTAB - (N-cetyl-N,N,N, trimethyl ammonium bromide, $\mathbf{C_{19}H_{42}BrN}$)

*CPCl - (Cetyl pyridinium chloride , $\mathbf{C_{21}H_{38}ClN.H_2O}$)

Surfactants are used to control the morphology of the material during reaction. This synthesis of Zno in presence of different surfactants can be summarized as:

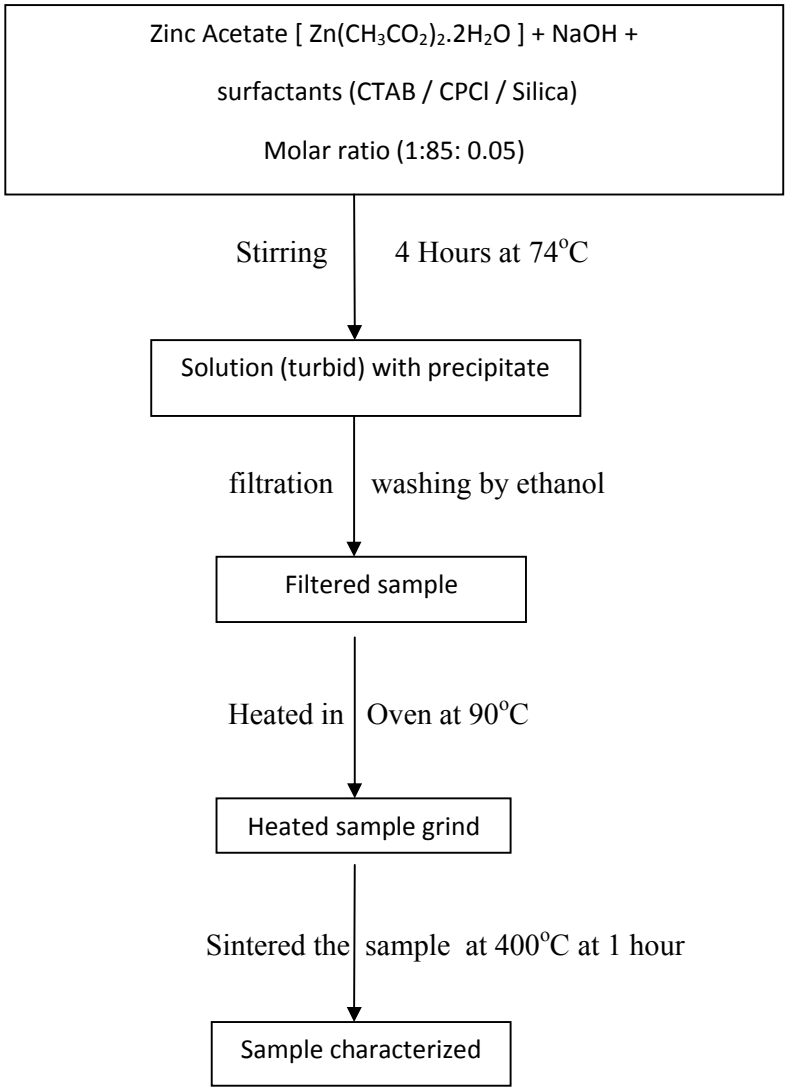

❖ Doping of Didymium (Di):

➢ Sample 6- Zno: 0.5% Di:

Chemical name	Chemical formula	Mole required	Material Taken
Zinc acetate	$(C_2H_3O_2)_2Zn.2H_2O$	0.02	4.14 gm
Sodium hydroxide	NaOH	0.08	3.20 gm
Ethanol	C_2H_5OH	---	100 ml
Didymium	Di	0.5	0.25 gm

➢ Sample 7- Zno: 1% Di:

Chemical name	Chemical formula	Mole required	Material Taken
Zinc acetate	$(C_2H_3O_2)_2Zn.2H_2O$	0.02	3.89 gm
Sodium hydroxide	NaOH	0.08	3.20 gm
Ethanol	C_2H_5OH	---	100 ml
Didymium	Di	1.0	0.5 gm

➢ Sample 8- Zno: 3% Di:

Chemical name	Chemical formula	Mole required	Material Taken
Zinc acetate	$(C_2H_3O_2)_2Zn.2H_2O$	0.02	2.89 gm
Sodium hydroxide	NaOH	0.08	3.20 gm
Ethanol	C_2H_5OH	---	100 ml
Didymium	Di	3.0	1.50 gm

➢ Sample 9- Zno: 5% Di:

Chemical name	Chemical formula	Mole required	Material Taken
Zinc acetate	$(C_2H_3O_2)_2Zn.2H_2O$	0.02	1.89 gm
Sodium hydroxide	NaOH	0.08	3.20 gm
Ethanol	C_2H_5OH	---	100 ml
Didymium	Di	5.0	2.5 gm

ZnO was doped with rare earth material didymium (a mixture of neodymium and praseodymium). Didymium is a naturally occurring element with major constituent Nd and Pr.

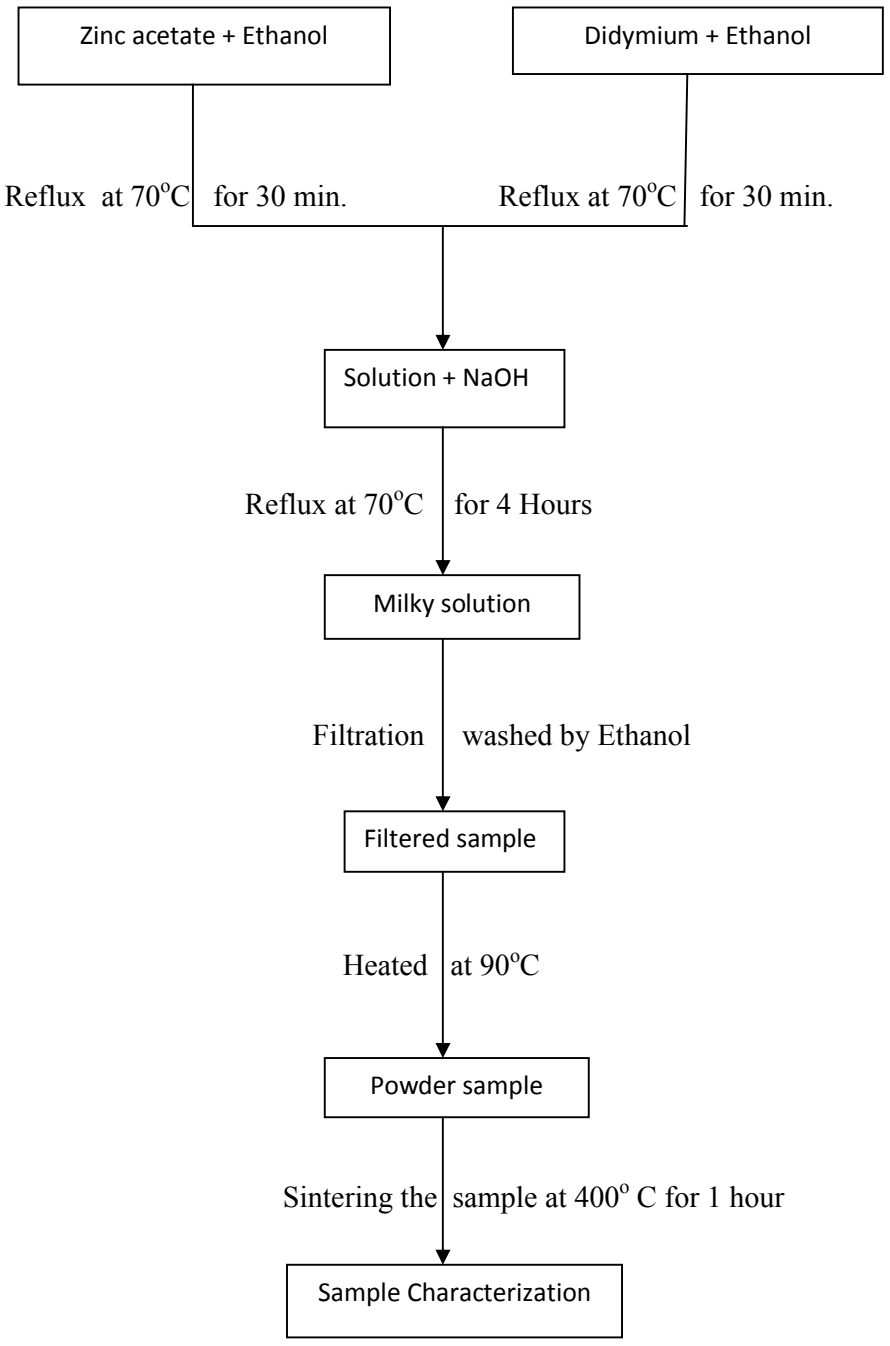

❖ Doping of silver (Ag):

➢ Sample 10- Zno: 1.0% Ag:

Chemical name	Chemical formula	Mole required	Material Taken
Zinc acetate	$(C_2H_3O_2)_2Zn.2H_2O$	0.02	3.89 gm
Sodium hydroxide	NaOH	0.08	3.20 gm
Ethanol	C_2H_5OH	---	100 ml
Silver nitrate	$AgNO_3$	1.0	0.50 gm

➢ Sample 11- Zno: 3% Ag:

Chemical name	Chemical formula	Mole required	Material Taken
Zinc acetate	$(C_2H_3O_2)_2Zn.2H_2O$	0.02	2.89 gm
Sodium hydroxide	NaOH	0.08	3.20 gm
Ethanol	C_2H_5OH	---	100 ml
Siver Nitrate	$AgNO_3$	3.0	1.50 gm

In another experiment ZnO was doped with silver (Ag). Silver nitrate ($AgNo_3$) was mixed with zinc acetate in presence of ethanol. $Zn_{1-x}Ag_xO$ (where x = 0.1, 0.3) was prepared in nano powder form.

Experimental procedure can be shown as:

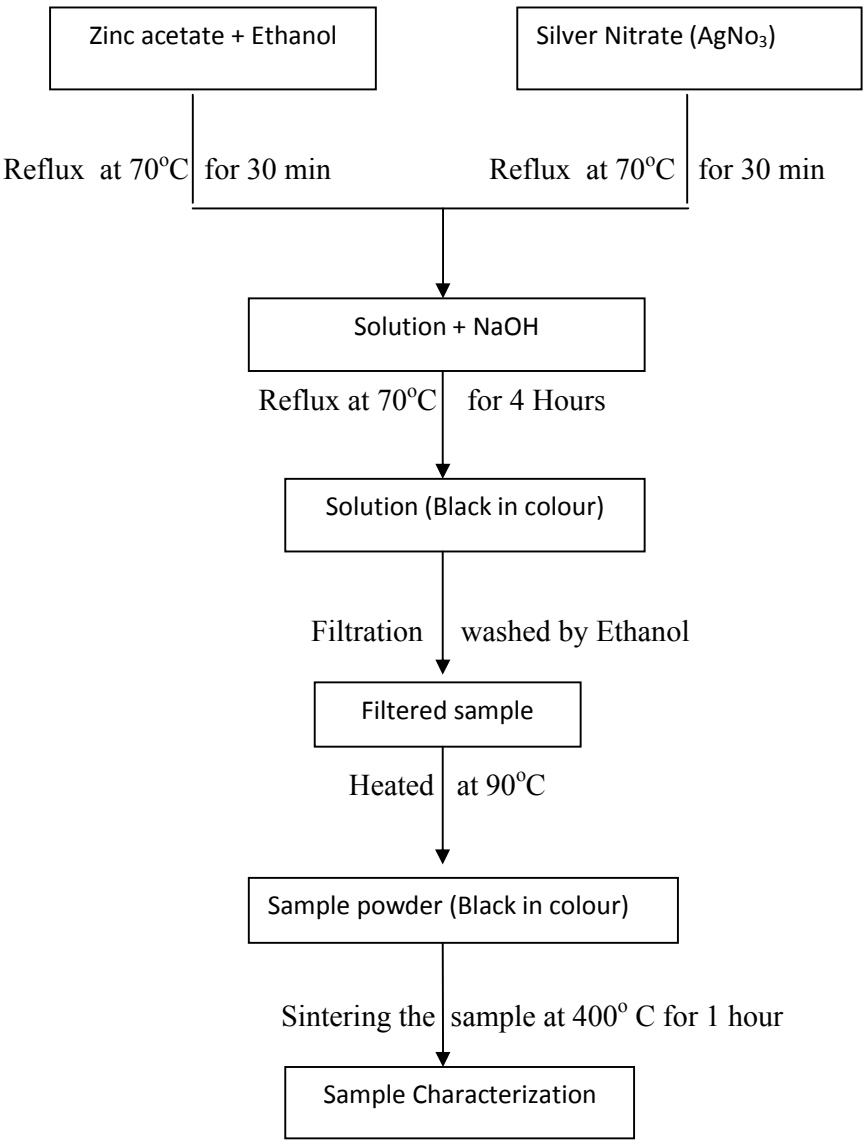

2.3 Characterization techniques

2.3.1 X-ray Diffraction

X-ray diffraction (XRD) is a versatile, non-destructive technique used for qualitative and quantitative analysis of a crystalline materials. This experimental technique has been used to determine the overall structure of bulk solids, including lattice constants, identification of unknown materials, orientation of single crystals, orientation of polycrystalline, stress, texture, films thickness etc. In this study a powder diffraction system with Cu-Ka x-ray tube (λ=1.54056 A^0) A) was used. The x-ray scans were performed between 2θ values of 30° and 80° with a typical step size of about 0.1° [39,40].

2.3.1.1 Generation of X -ray

X-rays are short-wavelength, high energy electromagnetic radiation, having the properties of both waves and particles. They can be described in terms of both photon energy (E) or wavelength, λ (lambda – the distance between peaks) and frequency ν (nu – the number of peaks passing a point in a unit of time).The relation between energy, frequency or wavelength in the case of photon is:

$$\mathbf{E = h\nu = \frac{\quad}{\quad}} \qquad 2.1$$

Substituting the values of the constants above in equation yield the following relationship

$$\boldsymbol{\lambda = \frac{\cdot}{(\quad)}} \qquad 2.2$$

X-rays are produced whenever high energy electrons strike with metal target, any x-ray tube must contain (a) a source of electron (b) a high accelerating voltage (c) a metal target. All x-ray tubes contain two electrodes, an anode (the metal target) usually maintained, at ground potential, and a cathode mainted, at negative potential, normally of order of 30KV to 50KV for the diffraction work. Interaction that occur between the beam (i.e. electron) and target will result in a loss of energy. A continuous spectrum is formed when the high energy electrons are slowed down rapidly by multiple collisions with the anode material, which give rise to white radiation, or so called Bremsstrahlung.

The continuous spectrum is formed due to rapid deceleration of the electrons hitting the target, as mentioned above, but not every electron decelerates in the same way, some stop in one impact and release all their energy at once, while other deflect this way and that when

they encounter atoms of the target, successively losing fractions of their total kinetic energy until is all spent. Those electrons which are stopped in one impact produce photons of maxim energy (wavelength) equal to the energy loss [41].

2.3.1.2 Bragg's Law

Since atoms are arranged periodically in a lattice, x-rays scattered from a crystalline solid can constructively interfere, producing a diffracted beam through these atoms. In 1912, W. L. Bragg recognized a predictable relationship among several factors. These factors are combined in Bragg's law:

$$n\lambda = 2d \sin\Theta \qquad (2.3)$$

n = an interger-1, 2, 3….etc [n=1 for our calculations]

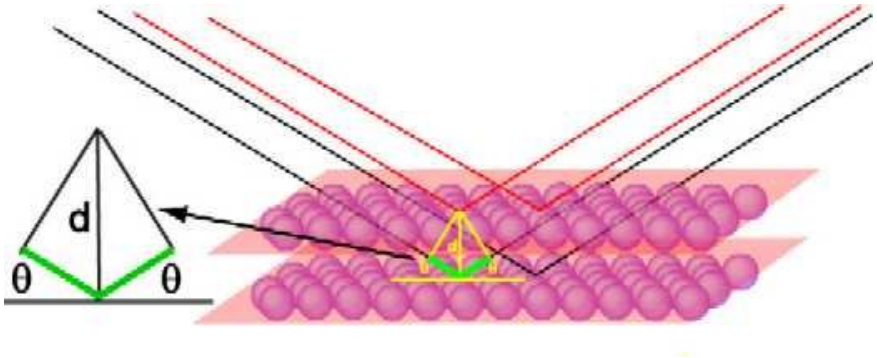

Figure 2.2: Bragg's diffraction condition.

λ = the wavelength of the incident X-radiation, symbolized by the Greek letter lambda and, in our case, equal to 1.54 angstroms. d = the distance between similar atomic planes in a mineral (the interatomic spacing) which we call the d-spacing and measure in angstroms.

θ = the diffraction angle in degree The Ewald sphere construction provides a relation between Bragg's law and the reciprocal space mapping (RSM). RSM is a valuable tool during ω-2θ scan, when strain field exist within the grain. Basically, RSM build on wave vector translation into reciprocal space. The radius of the Ewald sphere is equal to wave vector of the incident X-ray $|K| = 2\pi/\lambda$, which is drawn in such a way that it end at the origin of the reciprocal space as shown in figure 3.3. The diffracted beam with wave vector K_{diff} is determined from $K_{diff} = K_{inc} + G$, where G is the scattering vector, which is normal to the set of plane involved in scattering event. The diffraction condition is fulfilled only if there is a reciprocal lattice point on the Ewald sphere surface at G.

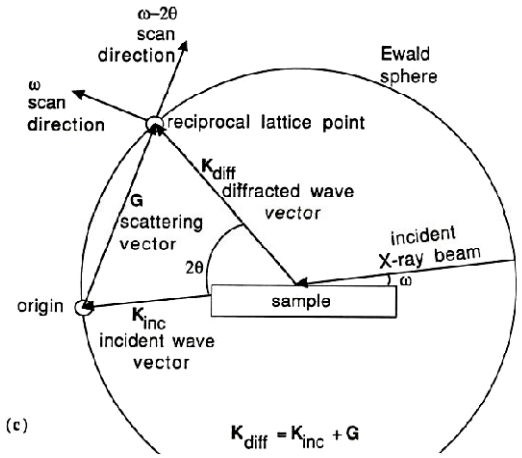

Figure 2.3: Schematic of asymmetric reflection in reciprocal space.

When the sample is grown one or more epilayers on a substrate, the RSM of the structure will consist of the points corresponding both from to the diffraction from the substrate planes as well as from the epilayer planes. In this case, the difference in the interplanar distance and orientation of each epilayer relative to the substrate will lead to different position of the respective reciprocal lattice points relative to the substrate and relative to reciprocal space coordinate system. The intensity distribution and shape of the RSM provide structural information about e.g. crystal quality (FWHM), film/substrate mismatch, stress-state and lattice parameters.

2.3.1.3 Crystallite size measurement

Phase identification using x-ray diffraction depends on the positions of the peaks in a diffraction profile as well as the relative intensities of these peaks to some extent. Another aspect of the diffraction from material is the importance to consider how diffraction peaks are changed by the presence of various types of defects such as small number of dislocations in crystals with dimensions of millimetres. Small size of grain size can be considered as another kind of defect and can change diffraction peak widths. Very small crystals cause peak broading. The crystallite size is easily calculated as a function of peak width (specified as the full-width at half maximum peak intensity (FWHM)), peak position and wavelength.

Scherrer's formula

Suppose that the crystal has a thickness d measured in a direction perpendicular to a particular set of Bragg planes (Figure2.4). Let there be (m + 1) planes in this set. Define the

Bragg angle as a variable and let θ_B be the angle which exactly satisfies Bragg's law for the particular values of λ and d involved, or

$$n\lambda = 2d \sin\Theta \qquad 2.4$$

In figure 3.4, rays **A**, **D**… **M** make exactly this angle with the diffraction planes. Incident x-rays that make angles only slightly different from θ_B, produce incomplete destructive interference. Ray **B**, for example, makes a slightly larger angle θ_1 such that ray **L**' from the mth plane below the surface is (m + 1) wavelengths out of phase with **B'**, the ray from the surface plane. The intensity of the beam diffracted at an angle $2\theta_1$ is therefore zero. It is also zero at an angle $2\theta_2$, where θ_2 is such that ray **N'** from the mth plane below the surface is (m - 1) wavelengths out of phase with ray **C**' from the surface plane. This defines, therefore, the two limiting angles, $2\theta_1$ and θ_2, at which the diffracted intensity must drop zero.

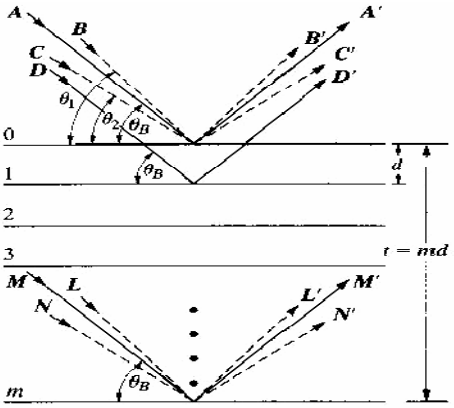

Figure 2.4: Effect of crystal size on diffraction.

The curve of diffracted intensity vs. 2θ will thus have the form of Figure 2.5a in contrast to Figure 2.5b, which illustrates the hypothetical case of diffraction occurring only at the exact Bragg angle.

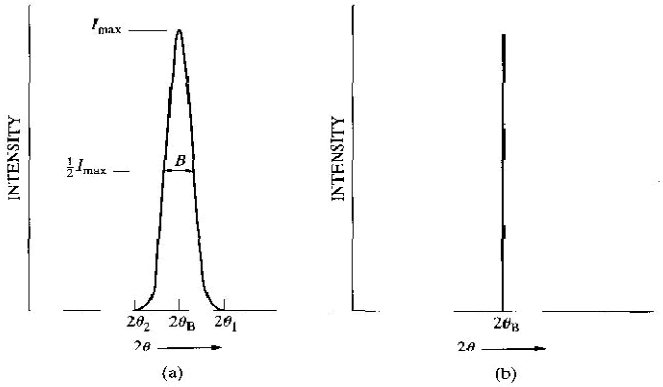

Figure 2.5: Effect of fine crystallite size on diffraction curves.

The width of the diffraction curve of Figure 2.5a increases as a thickness of the crystal decreases, because the angular range ($2\theta_1$ - $2\theta_2$)) increases as m decreases. The width B is usually measured, in radians, at an intensity equal to half the maximum intensity (FWHM). Therefore

$$B = ½ (2\theta_1 - 2\theta_2) = \theta_1 - \theta_2$$

The path-difference equations these tow angles are similar, But related to entire thickness of the crystal rather than to the distance between adjacent planes:

$$2\delta \sin\theta_1 = (m+1)\,\lambda,$$

$$2\delta \sin\theta_2 = (m-1)\,\lambda$$

By subtraction,

$$\delta (\sin\theta_1 - \sin\theta_2) = \lambda$$

$$2\delta \cos \frac{\theta \quad \theta}{\quad} \sin \frac{\theta \quad \theta}{\quad} = \lambda$$

But θ_1 and θ_2 are both very nearly equal to the θ_B, so that

$$\theta_1 + \theta_2 = 2\theta_B \text{ (approx)}$$

$$\sin \frac{\theta \quad \theta}{\quad} = \frac{\theta \quad \theta}{\quad} \text{ (approx)}$$

Therefore

$$2\delta \frac{\theta \quad \theta}{\quad} \cos\theta_B = \lambda$$

Or,

$$\delta = \frac{\lambda}{\theta}$$

A more exact treatment of the problems,

$$\delta = \frac{\cdot\ \lambda}{\theta} \qquad 2.5$$

This is known as Scherrer's formula. It is used to estimate the size of very small crystals from measured width of their diffraction curves. Note that whether a value of 0.9 or 1 is used depends on shapes of the crystallites assumed to be sample.

2.3.1.4 Determination of lattice parameters :

For the wurtzite structure the interplanar distance of (hkl) plane is related to the lattice parameters a and c via the Miller indices hkl:

$$\frac{}{} = - \frac{}{} + \frac{}{} \qquad 2.6$$

For the lattice parameters determination for a c-plane oriented film includes a measurement

of d_{100} in order to determine the c lattice parameter, and for the determination of a lattice from a second measurement of with either h or k different from zero [42].

2.3.2 Scanning Electron Microscopy (SEM):

Scanning electron microscopy (SEM) is basically a type of electron microscope. SEM is used for various purposes;

- Topographic studies.
- Microstructure analysis.
- Elemental analysis if equipped with appropriate detector (energy/wavelength dispersive x-rays).
- Chemical composition.
- Elemental mapping.

Fig. 2.6: Image of SEM and Edax Set up

In SEM, Primary electrons are thermonically or field emitted by a cathode filament (W or LaB)) or a filed emission gun (W-tip) and after that accelerated with high energy typically 1-30KeV. The electron beam is steered with scanning coils over the area of the interest. Upon interaction with material, the primary electrons decelerate as well as losing his energy, transfer it inelastically to other atomic electron and to the lattice. Due to continuous scattering events the primary beam spread up with different energies depending on source origin as shown in figure. 2.7a. the interaction volume with the various electrons emitted and their respective energy is shown in figure 2.7 b.

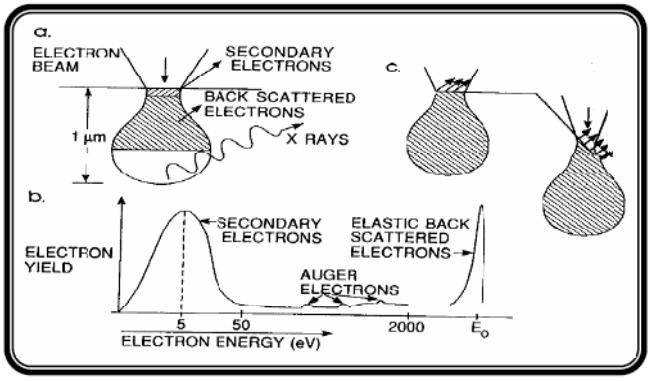

Figure 2.7: (a) Electron interactions with the surface during bombardment. (b) Type of electrons and corresponding energies of the emitted electrons after element interaction. (c) Effect of surface topography on electron emission .

Secondary electrons (1-50eV) are mostly used for the imaging the topographically contrast and reproduce the surface. High energy elastically backscattered electrons depends on the atomic number (Z) of the element, which is useful to obtain Z-constrat. X-ray characteristic can be used to qualitatively and quantitatively analyze the elemental composition and distribution in the sample.

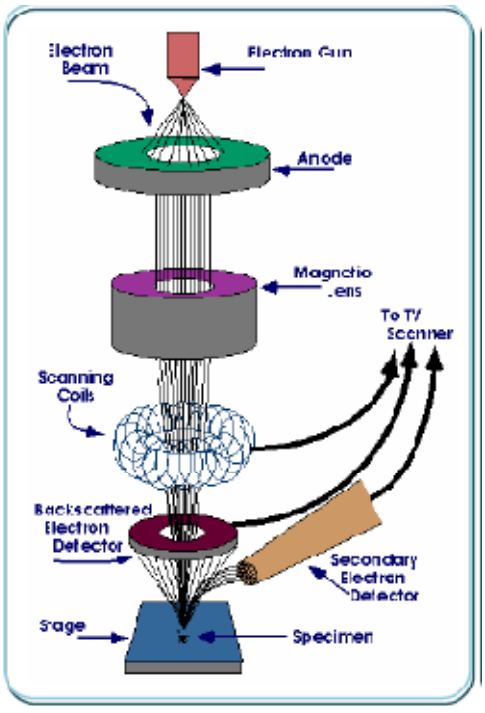

Figure 2.8: Schematic illustration of the SEM.

2.3.2.1 SEM setup

The experimental setup consists of an electron gun, column, scanning system, substrate chamber, detectors.

Electron gun

It is based on the thermal emission. The electron source is commonly a tungsten (W) or lanthanum hexaboride (LaB_6) tip. Electrons are emitted during heating.

Column

The column consists of two electromagnetic lenses acting on the electron beam. The first lens, the condenser lens produces most of the beam demagnification, while the second, objective lens focuses the beam onto the sample. In column, a beam shaper called stigmator, the stigmator can create a magnetic field around the beam to restore it in a circular cross section.

Scanning system

To get image on the display the beam should be scanned over the specimen and the display tube. Information from any point on the sample can then reproduced in the same relative position on the display.

Substrate chamber

The substrate holder depends on the different size and shape of the sample. The sample can be moved in three dimensions, as well as rotated and titled.

Detector

The most detector types used for secondary electrons are the scintillation detector. It can be used for primary electrons.

X-ray detector.

Spectrometers for detection and analysis of X-ray s are based on either of two principles.

- Wavelength dispersive X-ray (WDX); determines the wavelength of the X-rays.
- Energy dispersive X-ray (EDX); determine the energy of the X-rays.

2.3.4 Fourier transformation IR Spectroscopy

FT-IR stands for Fourier Transform Infrared, the preferred method of infrared spectroscopy. The prepared samples were characterised by FTIR spectroscopy. The experimental set up shown is in figure 2.9. In infrared spectroscopy, IR radiation is passed through a sample. Some of the infrared radiation is absorbed by the sample and some of it is

passed through (transmitted). The resulting spectrum represents the molecular absorption and transmission, gives information of type of bonding in the sample. This makes infrared spectroscopy useful for several types of analysis.

• FTIR can identify unknown materials

• FTIR can determine the quality or consistency of a sample

• FTIR can determine the amount of components in a mixture.

The original infrared instruments were of the dispersive type. These instruments separated the individual frequencies of energy emitted from the infrared source. This was accomplished by the use of a prism or grating. A grating is a more modern dispersive element which better separates the frequencies of infrared energy. The detector measures the amount of energy at each frequency which has passed through the sample. This results in a spectrum which is a plot of intensity vs. frequency.

Figure 2.9: Fourier transforms infrared (FTIR) spectrometry

Fourier Transform Infrared (FT-IR) spectrometry was developed in order to overcome the limitations encountered with dispersive instruments. The main difficulty was the slow scanning process. A method for measuring all of the infrared frequencies simultaneously, rather than individually, was needed. A solution was developed which employed a very simple optical device called an interferometer. The interferometer produces a unique type of signal which has all of the infrared frequencies “encoded” into it. The signal can be measured very quickly, usually on the order of one second. Thus the time element per sample is reduced to a matter of a few seconds rather than several minutes.

2.3.5 Energy dispersive X-ray spectroscopy

Energy dispersive X-ray spectroscopy (EDS, EDX or EDXRF) is an analytical technique used for the elemental analysis or chemical characterization of a sample. It is one of the variants of XRF. As a type of spectroscopy, it relies on the investigation of a sample through interactions between electromagnetic radiation and matter, analyzing x-rays emitted by the matter in response to being hit with charged particles. Its characterization capabilities are due in large part to the fundamental principle that each element has a unique atomic structure allowing x-rays that are characteristic of an element's atomic structure to be identified uniquely from each other.

To stimulate the emission of characteristic X-rays from a specimen, a high energy beam of charged particles such as electrons or protons (see PIXE), or a beam of X-rays, is focused into the sample being studied. At rest, an atom within the sample contains ground state (or unexcited) electrons in discrete energy levels or electron shells bound to the nucleus. The incident beam may excite an electron in an inner shell, ejecting it from the shell while creating an electron hole where the electron was. An electron from an outer, higher-energy shell then fills the hole, and the difference in energy between the higher-energy shell and the lower energy shell may be released in the form of an X-ray. The number and energy of the X-rays emitted from a specimen can be measured by an energy dispersive spectrometer. As the energy of the X-rays are characteristic of the difference in energy between the two shells, and of the atomic structure of the element from which they were emitted, this allows the elemental composition of the specimen to be measured.

The excess energy of the electron that migrates to an inner shell to fill the newly-created hole can do more than emit an X-ray. Often, instead of X-ray emission, the excess energy is transferred to a third electron from a further outer shell, prompting its ejection. This ejected species is called an Auger electron, and the method for its analysis is known as Auger Electron Spectroscopy (AES).

X-ray Photoelectron Spectroscopy (XPS) is another close relative of EDS, utilizing ejected electrons in a manner similar to that of AES. Information on the quantity and kinetic energy of ejected electrons is used to determine the binding energy of these now-liberated electrons, which is element-specific and allows chemical characterization of a sample. EDS is often contrasted with its spectroscopic counterpart, WDS (Wavelength-Dispersive X-ray Spectroscopy). WDS differs from EDS in that it uses the diffraction patterns created by light-matter interaction as its raw data. WDS has a much finer spectral resolution than EDS. WDS

also avoids the problems associated with artifacts in EDS (false peaks, noise from the amplifiers and microphonics. In WDS only one element can be analyzed at a time, while EDS gathers a spectrum of all elements, within limits, of a sample.

2.3.6 Thermo gravimetric analysis

Thermo gravimetric Analysis (TGA) is a type of testing that is performed on samples to determine changes in weight in relation to change in temperature. Such analysis relies on a high degree of precision in three measurements: weight, temperature, and temperature change. As many weight loss curves look similar, the weight loss curve may require transformation before results may be interpreted. A derivative weight loss curve can be used to tell the point at which weight loss is most apparent. Again, interpretation is limited without further modifications and deconvolution of the overlapping peaks may be required.

TGA is commonly employed in research and testing to determine characteristics of materials such as polymers, to determine degradation temperatures, absorbed moisture content of materials, the level of inorganic and organic components in materials, decomposition points of explosives, and solvent residues. It is also often used to estimate the corrosion kinetics in high temperature oxidation. The analyzer usually consists of a high-precision balance with a pan (generally platinum) loaded with the sample. The pan is placed in a small electrically heated oven with a thermocouple to accurately measure the temperature. The atmosphere may be purged with an inert gas to prevent oxidation or other undesired reactions. A computer is used to control the instrument.

Analysis is carried out by raising the temperature gradually and plotting weight against temperature. The temperature in many testing methods routinely reaches 1000°C or greater, but the oven is so greatly insulated that an operator would not be aware of any change in temperature even if standing directly in front of the device. After the data is obtained, curve smoothing and other operations may be done such as to find the exact points of inflection.

A method known as hi-res TGA is often employed to obtain greater accuracy in areas where the derivative curve peaks. In this method, temperature increase slows as weight loss increases. This is done so that the exact temperature at which a peak occurs can be more accurately identified. Several modern TGA devices can vent burnoff to a fourier-transform infrared spectrophotometer to analyze composition.

Chapter 3

Result & Discussion

RESULTS AND DISCUSSION

In this chapter we discuss results obtained from the X-ray diffraction, Scanning electron microscopy (SEM), FTIR, TGA and UV spectroscopy. The results are mainly divided in two parts (i) Structural and morphological analysis (ii) chemical analysis. Further we also calculated particle size, lattice constant and energy band gap of the synthesized samples. Finally we discussed the material physics behind the formation of such metal oxide complexes and the chemical and physical interaction between solvent and precursor used in the reaction.

3.1 Synthesis of ZnO in basic medium:

- **Structural and morphological analysis:**
  - **XRD Analysis:**

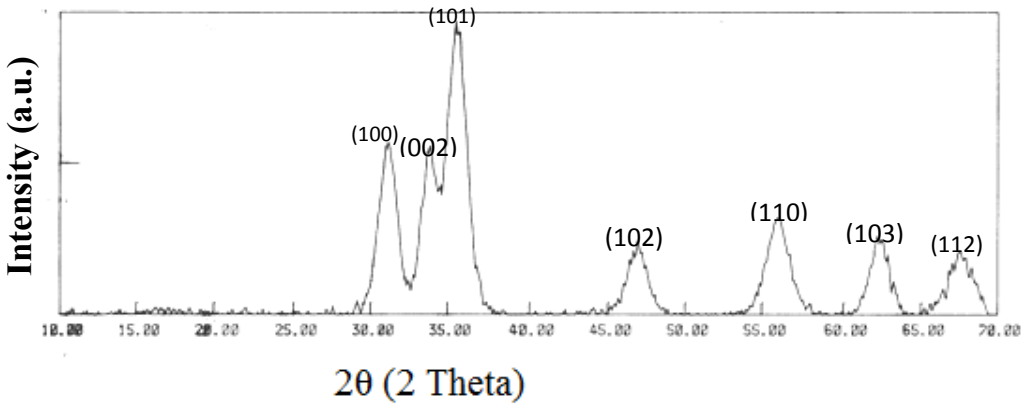

Fig. 3.1: XRD spectra of synthesized ZnO in basic medium

Figure 3.1 shows the XRD pattern of the ZnO, synthesized in basic medium. We observed that the sample is highly crystalline as evident from the XRD pattern in which broad peaks with high intensity extended over the 2θ scale. The peak observed at 2θ = 31.5^0, 33.76^0, 35.9^0, 47.23^0, 56.18^0, 62.2^0 and 67.6^0 correspondence to the lattice plane (100), (002), (101), (102), (110), (103) and (112) respectively, indicative of wurtzite hexagonal structure of ZnO. All the peaks are matched with standard JCPDS card no. 50664. The boarding of the peaks gives an idea about the small particle size of the synthesized ZnO.

Further the crystalline size D, corresponding to the (101) peak, was calculated by using the Scherrer's formula: D = 0.9 /B CosΘ, where , B, Θ are X-ray wavelength, full width at half maximum (FWHM) and Bragg diffraction angle respectively. The calculated particle size was 4.8 nm. Lattice constants were also calculated according to the position of the diffraction peak located at $2\theta = 35.9^0$, the values of lattice constants **a** and **c** obtained are 3.3 A^0 and 5.3 A^0 respectively. The lattice constants obtained are approximately equal to the standard value of **a** and **c**, 3.25A^0 and 5.2 A^0 respectively.

SEM micrographs:

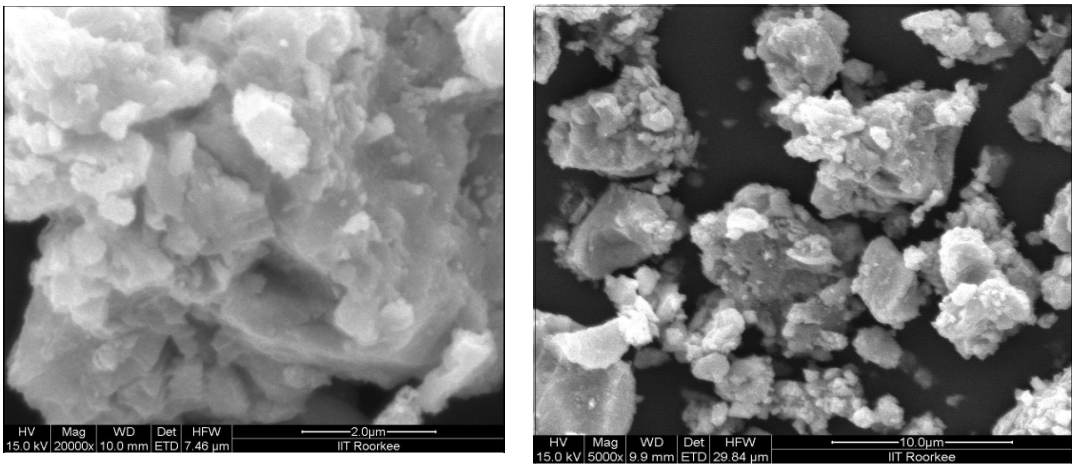

(a) **(b)**

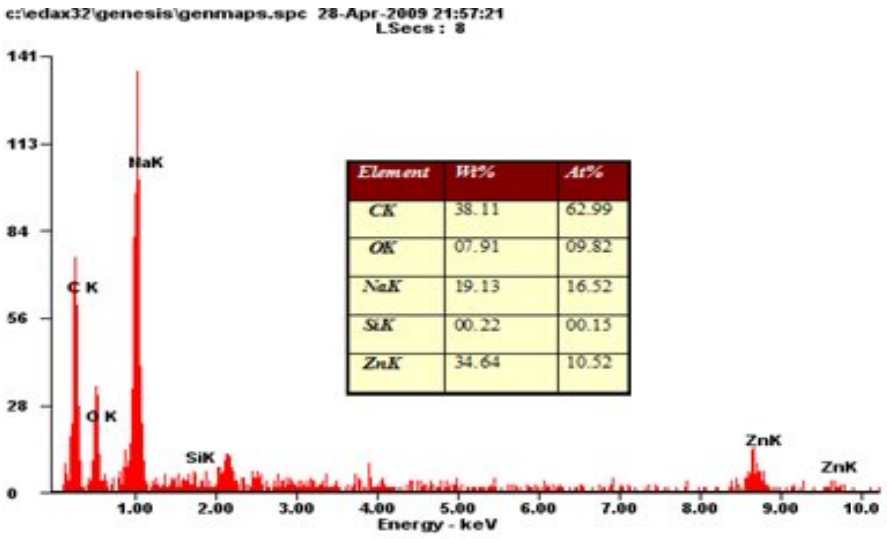

(c)

Fig 3.2: (a) SEM image at 20,000 X (b) SEM image at 5000X (c) EDX spectrum

SEM micrographs of the synthesized ZnO are shown in the figure 3.2 (a) and (b). From the figure it is quite evident that there is no definte morphology in the sample. It seems that the particles were agglomirated and form a cluster. As the particle size calculated from the XRD is in nano range we are not geting any exact information about the surface morpholgy of the sample from the SEM micrograph , because of the limitaion of our instruments upto micro range. The morpholgy observed in the sample not showing any hard grains which gives the idea that size of the particle is small and further needs to be characterized by Transmission elctron microscopy (TEM) to obtained exact morphology and size of the particles.

The EDX spectroscopy was performed to know the percentage of the elemnet present in the sample. The obtained percentage of the elements shown in figure 3.2(c). From the obtained data we found that the Zn and O were present in the higher percentage as shown in table, small percentage of other elements Na,Si,and C were also observed which may be due to residue of small amount of solvent and base materials used in the reaction.

Thermo gravimetrical analysis:

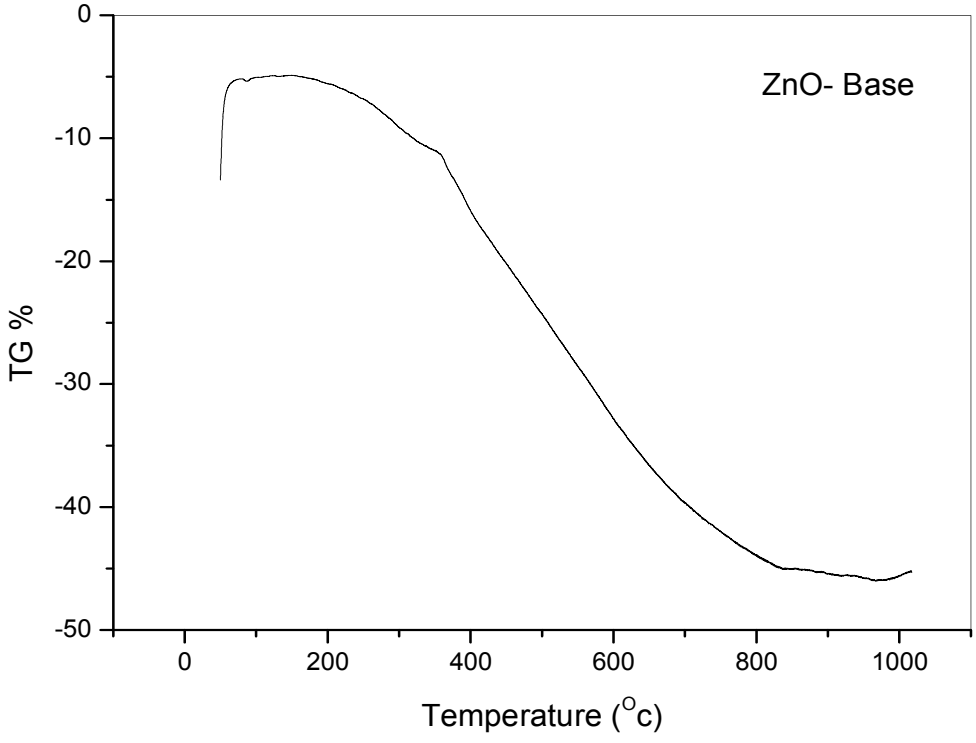

Fig 3.3: Thermal spectra of synthesized ZnO

Figure 3.3 shows the variation in weight loss in synthesized ZnO heated at the rate of 10^0C/min with increasing temperature. It is found that there is no significant change up to the 300^0C. The major loss in the weight of the sample at temperature 350^0 C was due to the evaporation of the lower melting point additive present. Losses were continuous up to the 800^0C and then become constant. From above result we conclude that the synthesized sample needs to be calcined at higher temperature to get product free from the residue and with higher crystallinity.

UV Spectroscopy:

The UV spectrum of the synthesized ZnO is shown in figure (3.4). only one peak observed in the UV region at wavelength 382.92 nm. The optical direct band gap calculated from the formula Eg = hc/ is 3.24 eV.

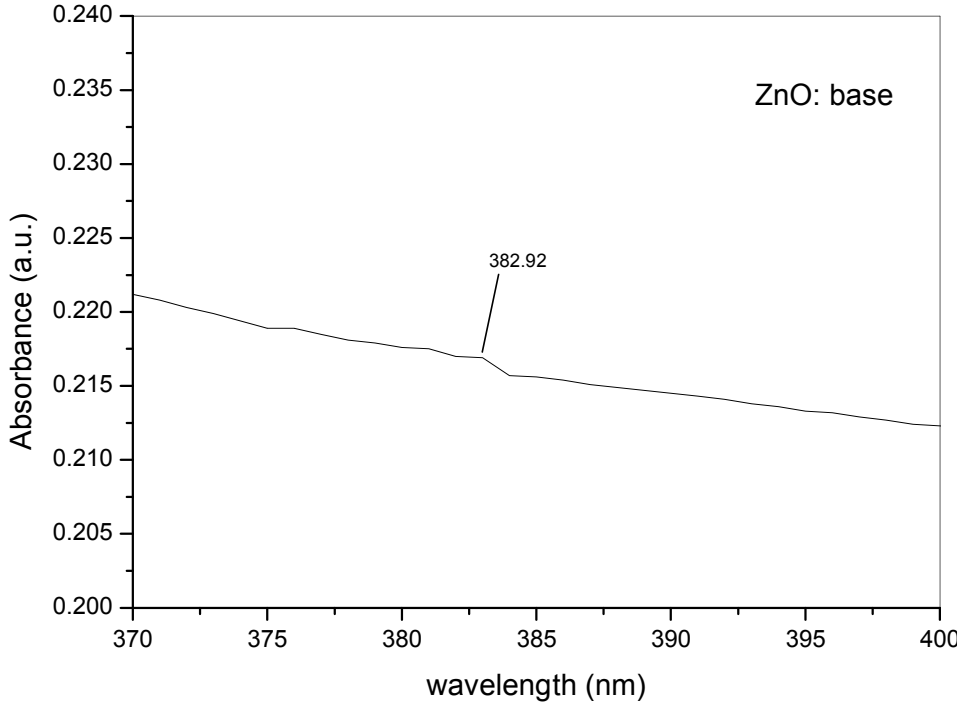

Fig 3.4: UV spectrum of the synthesized ZnO

3.2 Synthesis of ZnO in presence of different surfactants:

➢ Structural and morphological analysis before calcination:

- **XRD Analysis:**

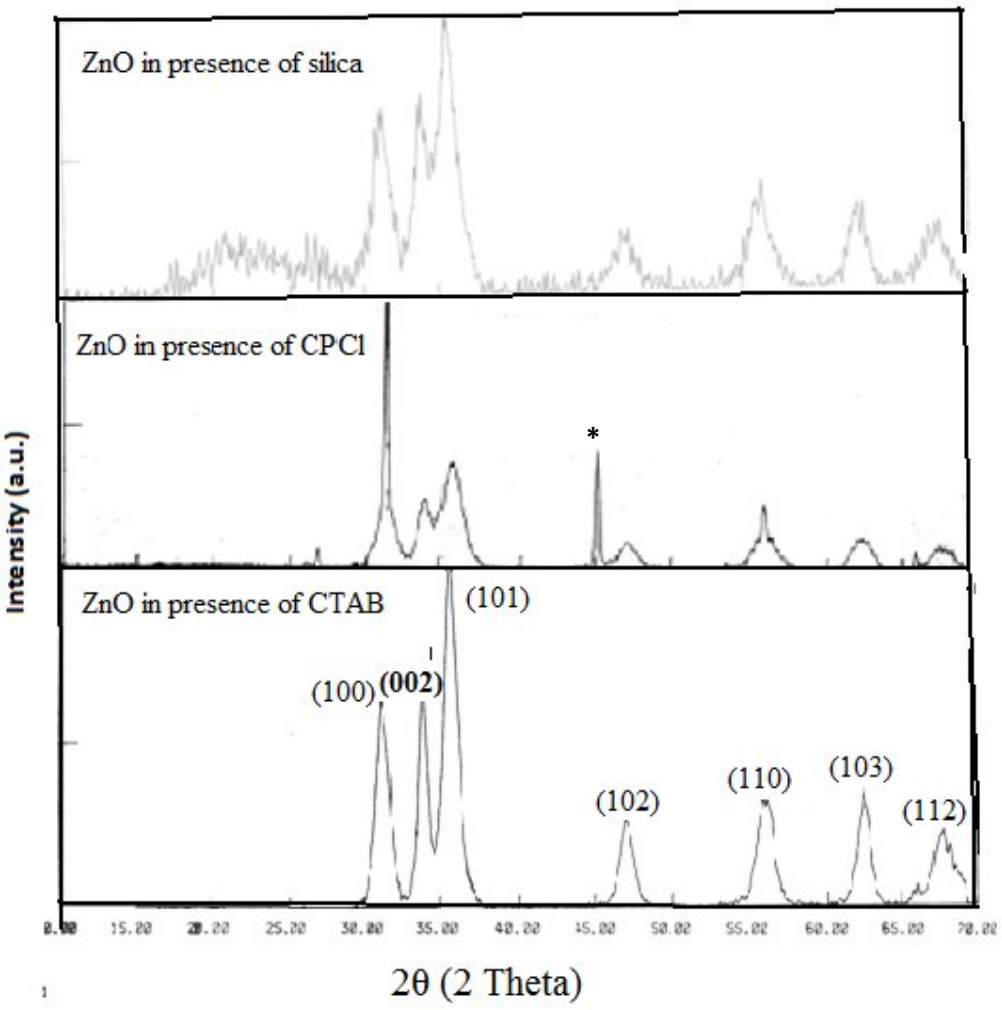

Fig (3.5): XRD spectra of ZnO synthesized in different basic medium.

The XRD pattern of the synthesized ZnO in the presence of the CTAB, CPCL and silica gel are shown in the figure 3.5. Highly intense peaks observed in the XRD pattern indicated that all the samples are well crystalline. The peaks obtained in all the samples at $2\theta = 31.5^0$, 33.7^0, 35.9^0, 47.23^0, 56.1^0, 62.2^0, 67.6^0 corresponds to the lattice planes (100), (002), (101), (102), (110), (103), (112) along with one characteristic peak (*) in the CPCl mediated sample. From above results we conclude that surfactants involved do not disrupting the crystal structure of ZnO. The characteristic peak in case of CPCl is due the presence of residue of solvent and

base materials. The calculated particle size of products (ZnO) obtained in the presence of CTAB, CPCl, Silica gel are 12.6 nm, 4.8 nm, 9.8 nm respectively.

SEM micrographs:

Before calcinations:

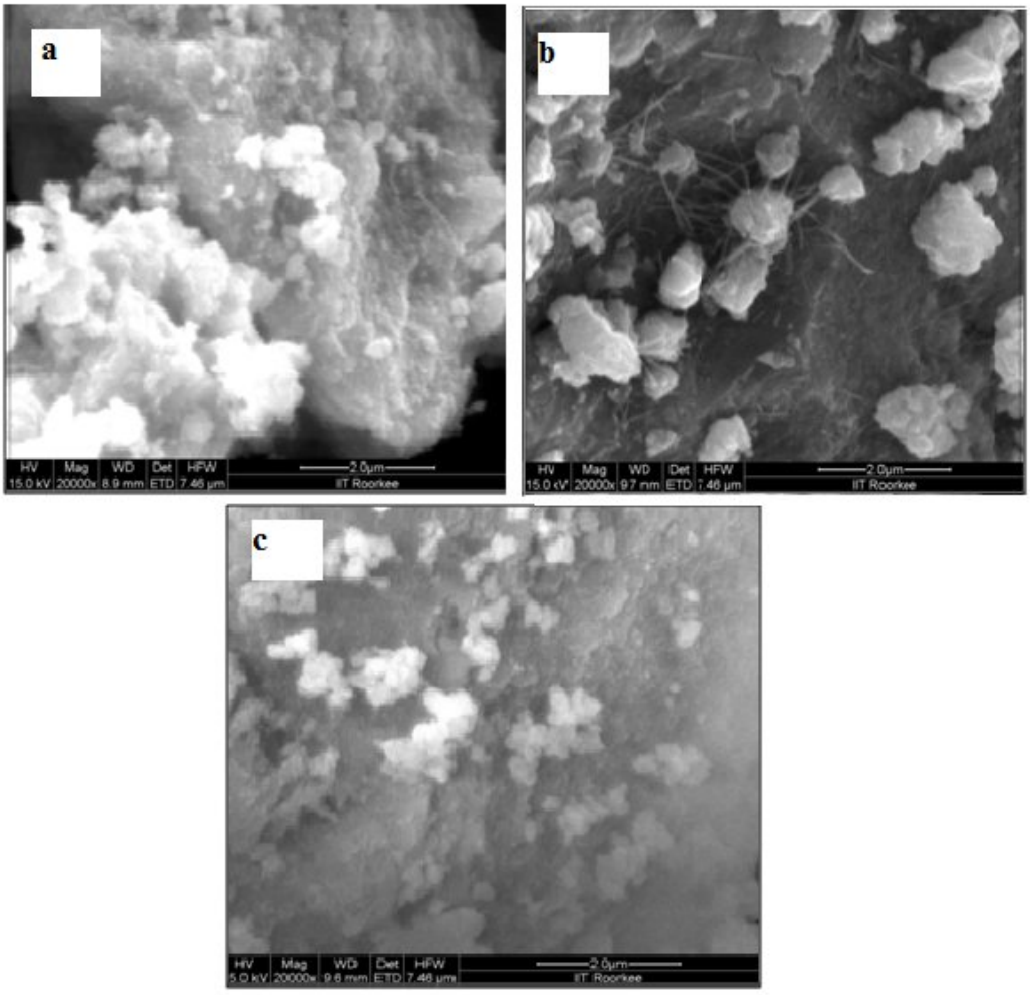

Figure 3.6: SEM images of the ZnO synthesized in presence of (a) CTAB, (b) CPCl and (c) Silica gel.

SEM images of the CTAB, CPCl and silica gel mediated samples are shown in figure 3.6. No difinte morphology obsereved in the case of sample synthesized by using CTAB and Si as shown in the SEM images in figure 3.6 a and c. It was obsereved that the particle are aglomirated and form the cluster . However in the presence of CPCl some growth of fibers were obsereved. From these SEM image, we are not getting any information which gives any

idea that surfactants play their role ot not. Further we need to charecterize our sample with TEM to find out the exact morphology and role of surfactants is they controlling the growth or not.

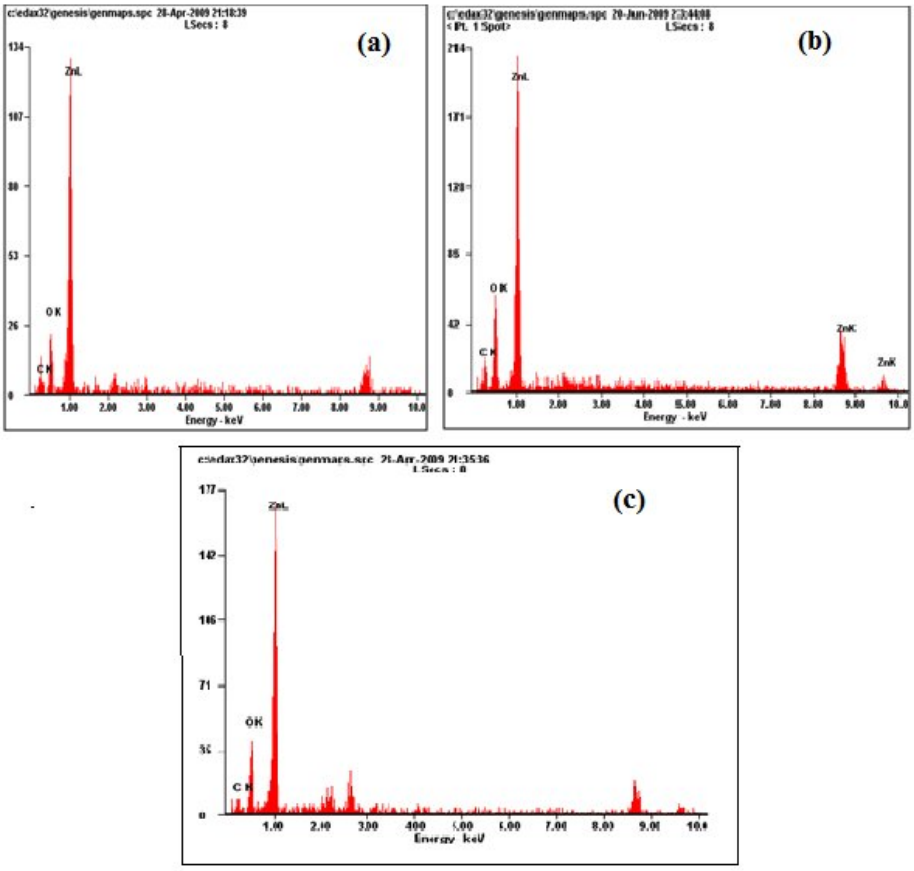

Figure 3.7: EDX spectra of the ZnO synthesized in the presence of (a) CTAB, (b) CPCl and (c) Silica gel.

The EDX spectra observed for these synstem is shown in figure 3.7. We observed that the sample contain Zn and oxygen contents along with small amount of carbon-C. However in the case of Silica gel mediataed sample small amount of Na and Si are presnet. Which is due to the Base (NaoH) and silica gel used in the medium.

Table -3.1: list of elements present in ZnO, synthesized in different surfactants:

Element	CTAB*		CPCl*		Silica gel	
	Wt%	At%	Wt%	At%	Wt%	At%
C K	19.21	46.09	13.67	34.86	17.36	33.04
O K	13.46	24.23	17.09	32.71	17.45	24.93
Na K	-	-	-	-	20.67	20.55
Si K	-	-	-	-	12.74	10.36
Zn K	67.33	29.68	69.24	32.43	31.78	11.11

*CTAB - (N-cetyl-N,N,N, trimethyl ammonium bromide, $\mathbf{C_{19}H_{42}BrN}$)

*CPCl - (Cetyl pyridinium chloride , $\mathbf{C_{21}H_{38}ClN.H_2O}$)

Thermo gravimetric analysis:

Figure 3.8 shows the variation in weight loss in synthesized ZnO in the presence of surfactants heated at the rate of 10^0C/min with increasing temperature. We observed that the

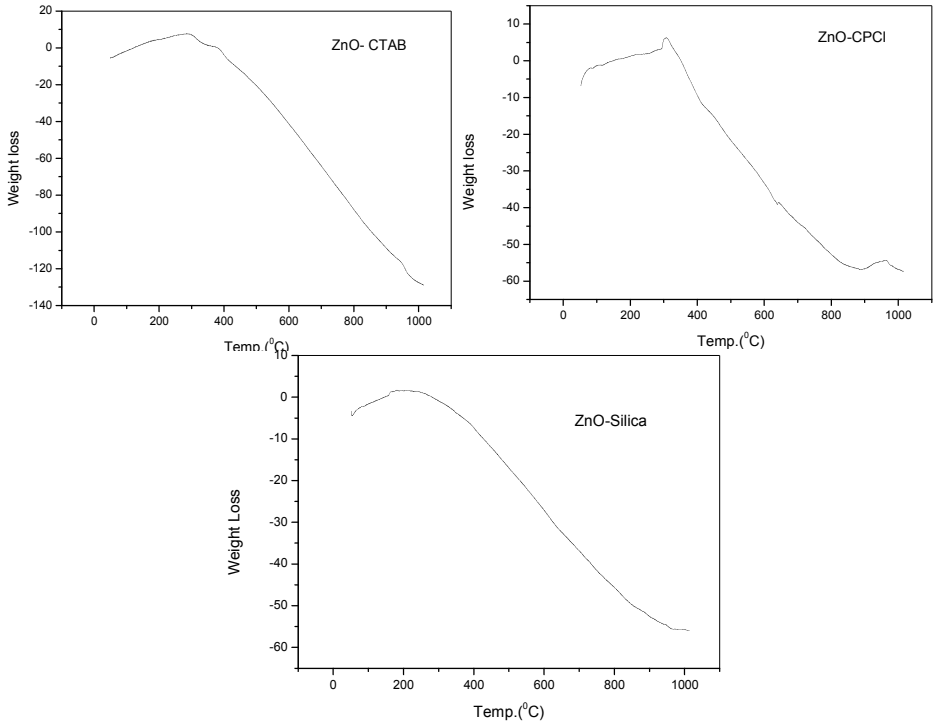

Fig 3.8: TGA of the ZnO synthesized in presence of different surfactants

sample follow the same trend as we observed one phase transition in the region 350^0-400^0 C in all cases, Which was due to the evaporation of lower melting additive from the complexes. At higher temperature all the samples showing the same trend without any phase change.

UV Spectrum:

The UV-visible spectra of the sample prepared in the presence of different surfactants are shown in figure 3.9. The absorbance peaks observed at 383nm, 384 nm, and 382 nm wavelengths the sample synthesized in the presence of CTAB, CPCl and Si respectively. The calculated optical band gaps were 3.23 eV, 3.23eV and 3.24 eV.

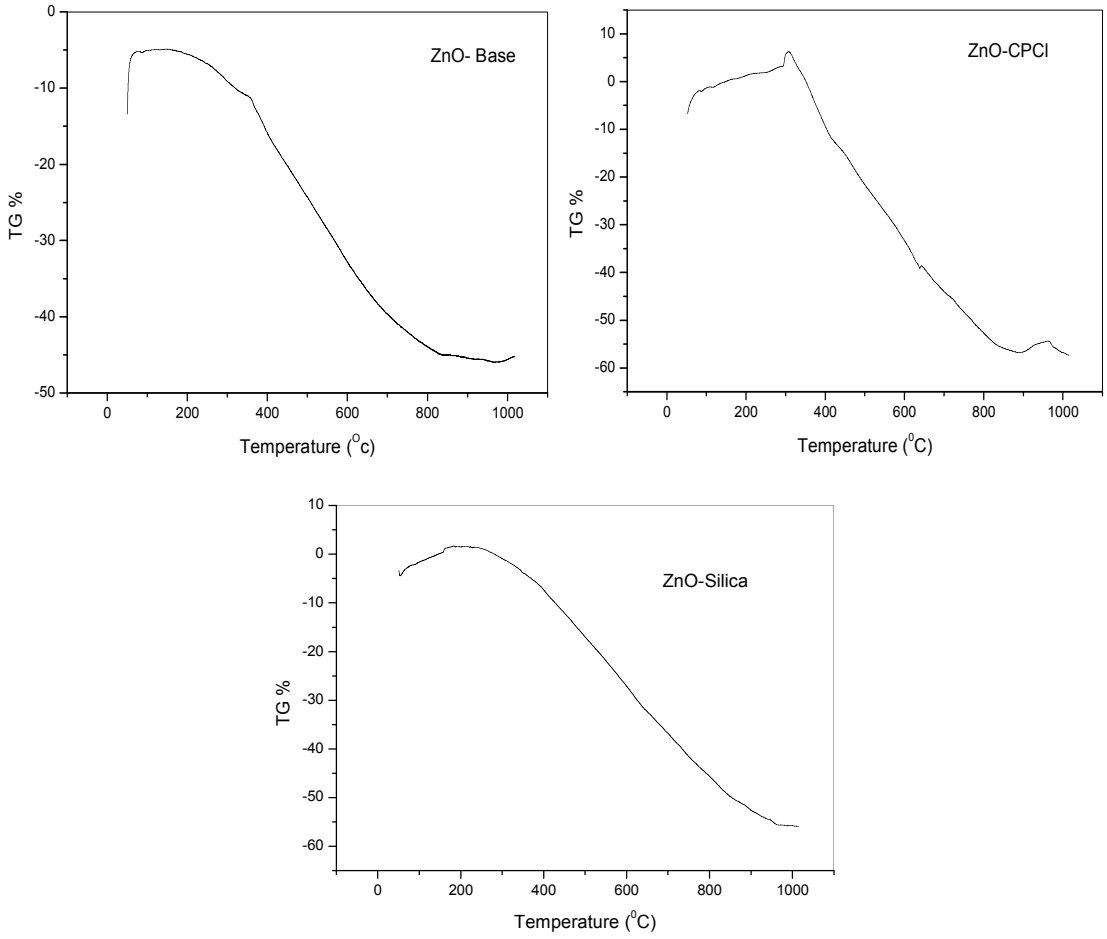

Fig.3.9: UV spectrum of the ZnO synthesized in presence of different surfactants.

After Calcination at 400^0 C for 1 hour:

SEM micrographs:

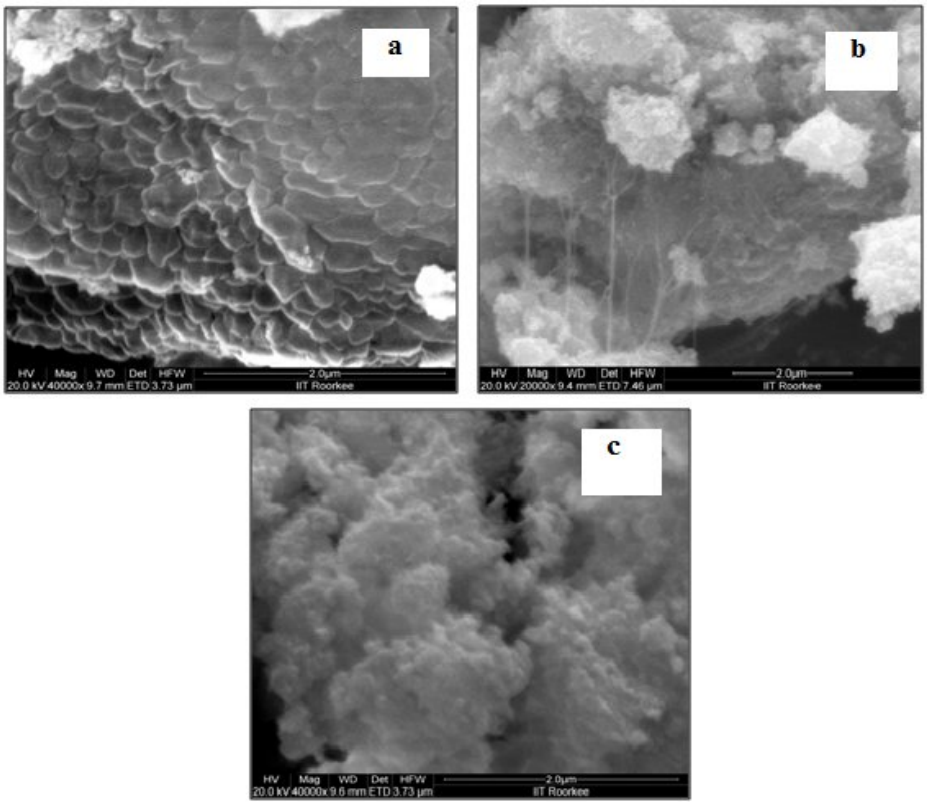

Fig 3.10: SEM images of the ZnO synthesized in the presence of (a) CTAB, (b) CPCl and (c) Silica gel after the calcinations at 400^0C for 1 hour.

The SEM images of ZnO synthesized in the presence of various surfactants (CTAB, CPCl and Si) calcined at 400^0C are shown in the figure 3.10. We found that the samples synthesized in the presence of CTAB shows the arrangement of the grain in well ordered manner, which may be due to the any reaction at higher temperature. Because such grains were not observed as pure synthesized sample before Calcinations. However, in case of CPCl and Si mediated samples no significant change was observed, the morphology were similar to uncalcined samples.

The EDX spectra of the calcined samples are shown in figure 3.11. We observed that after calcination, that the percentage of Zn and Oxygen contents were found to be higher and other impurity evaporates from the samples. However sample obtained from the CPCl shows the some impurity content also as listed in the table.

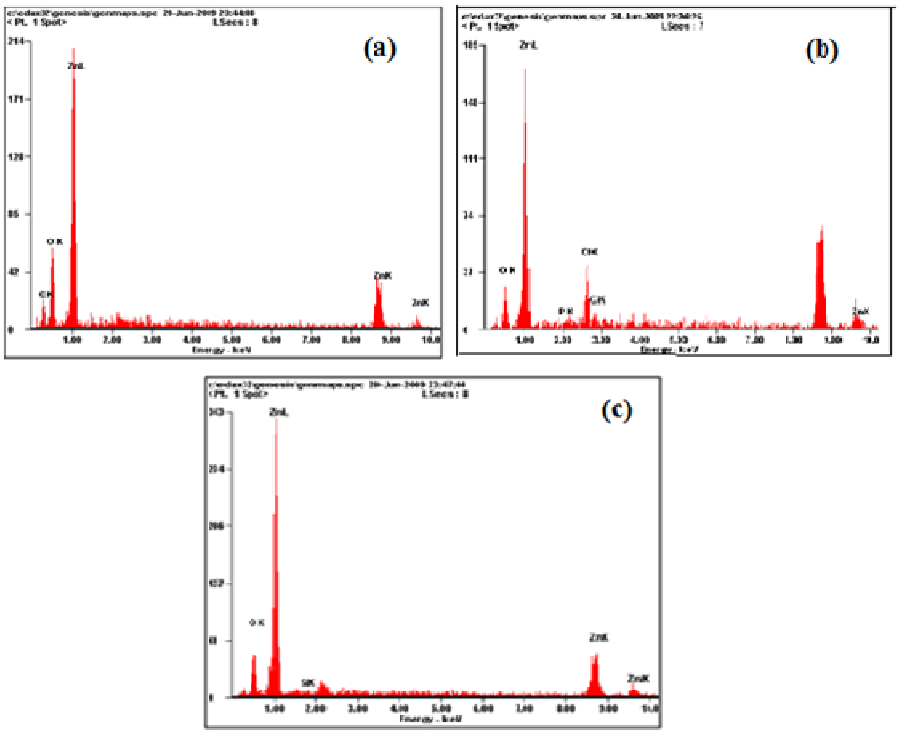

Fig 3.11: EDX spectra of the ZnO synthesized in presence of (a) CTAB, (b) CPCl and (c) Silica gel after the calcinations at 400^0C for 1 hour.

Table 3.2: List of elements present in ZnO synthesized in the presence of different surfactants after calcination

Element	CTAB*		CPCl*		Silica gel	
	Wt%	At%	Wt%	At%	Wt%	At%
C K	17.76	37.69	-	-	-	-
O K	25.15	40.06	14.44	38.52	18.43	47.63
Na K			-	-	-	-
Si K	-	-	-	-	00.91	01.34
Cl K	-	-	06.73	10.51	-	-
P K	-	-	01.15	01.59	-	-
Zn K	57.09	22.26	75.67	49.39	80.66	51.03

➢ Chemical analysis of ZnO synthesized in the presence of different surfactants:

- **FTIR spectra of synthesized Zno in presence of different surfactants:**

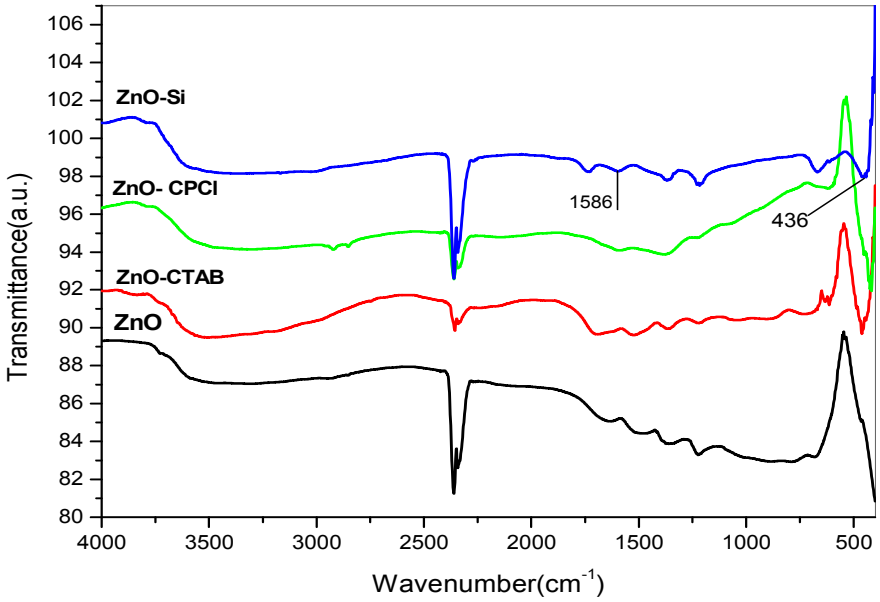

Fig. (3.12): FTIR of ZnO synthesizes in presence of different surfactants

- **FTIR of ZnO synthesised in different surfactants after calcination:**

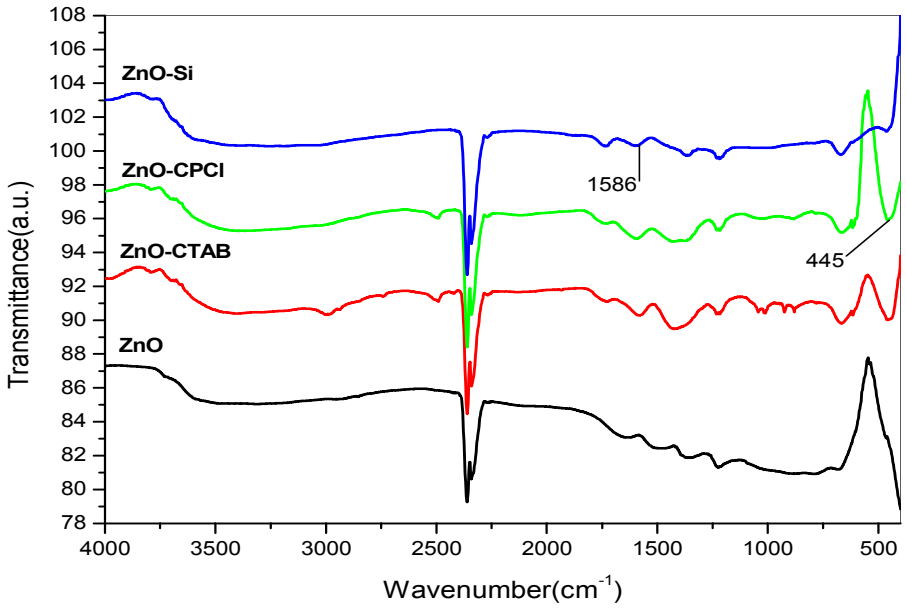

Fig. (3.13): FTIR of ZnO synthesizes in presence of different surfactants after calcinations at 400^{o} C

FTIR spectrum of the surfactants mediated synthesized ZnO sample is presented in the figure 3.12. The peak observed at 1586 cm^{-1} in all the samples corresponds to the COO^- group, which may be due to the small residue of zinc acetate used in reaction. Further peaks observed at 436 cm^{-1} indicative of the Zn – O stretching indicates the formation of ZnO.

The FTIR spectra of ZnO synthesized in the presence of CTAB, CPCl and Silica gel calcined at 400^0C is shown in figure 3.13. No significant change in the spectra was observed after calcination as evident from the spectra that all the peaks are at the same position.

3.3 Effect of different dopant on ZnO:

➢ 3.3.1 Effect of Didymium doping on ZnO:

- **XRD analysis:**

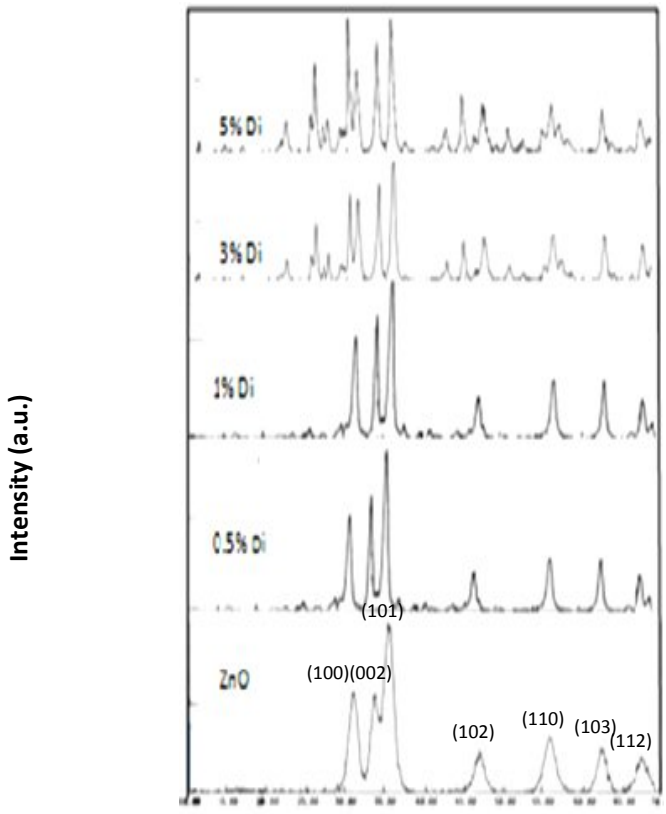

Fig (3.14): XRD spectra of Pure Zno, 0.5%, 1%, 3%, 5% Di doped ZnO

The XRD pattern of ZnO doped with Didymium at different concentration 0.5%, 1.0%, 3.0%, 5% is presented in figure 3.14. The peaks with the high intensity were observed in all the concentration gives an evidence about the crystallinity of samples. The peaks observed at 2θ = 31.5^0, 33.7^0, 35.9^0, 47.23^0, 56.18^0, 62.2^0, 67.7^0 indicative of lattice plane (100), (002), (101), (102), (110), (103), (112) matched with JCPDS card no. 50664 Up to 1% Di doping. we believe that Di ions fully fit in the valance site of Zn without disrupting the crystal structure , which also reflected from the lattice constant calculated from XRD pattern having same value as the standard value of a and c for ZnO. But at high concentration (3% and 5%) some additional peaks in the XRD pattern were observed along with ZnO peaks which indicate that at higher concentration dopant not going to the valance site and remain unreacted

- **SEM images of Didymium doped ZnO :**

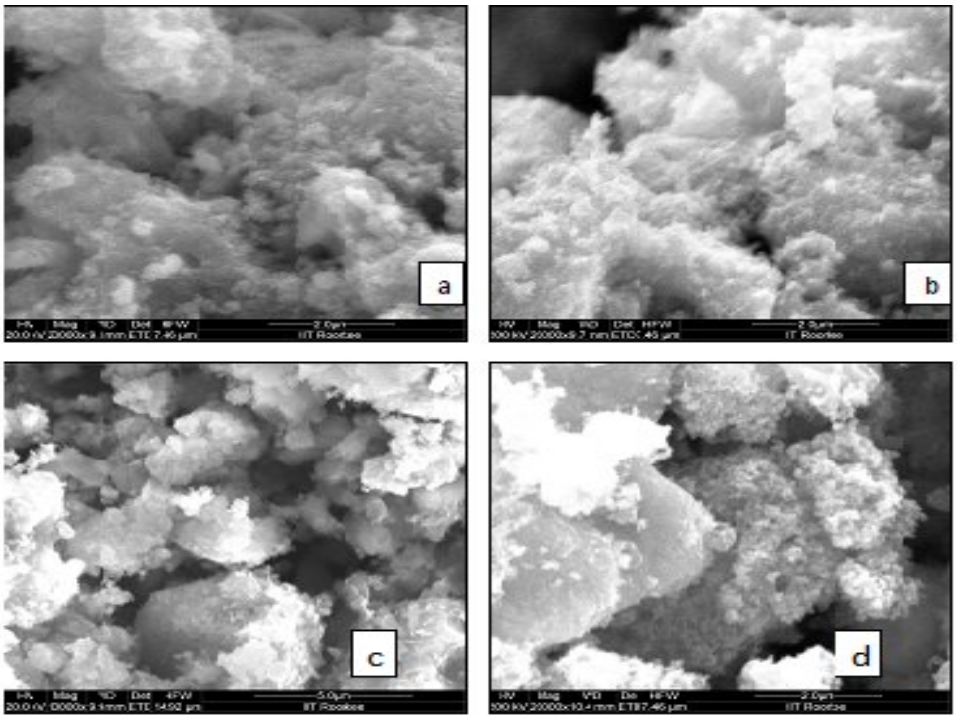

Fig (3.15): SEM images of (a) 0.5%, (b)1%, (c) 3%, (d) 5% Di doped ZnO at 20,000X

SEM images of the Di doped ZnO are shown in the figure3.13. No definite morphology was observed at any concentration. It appeared that the small grains were forming a cluster as evident from the SEM images (a), (b), (c) and (d) shown in figure 3.15.

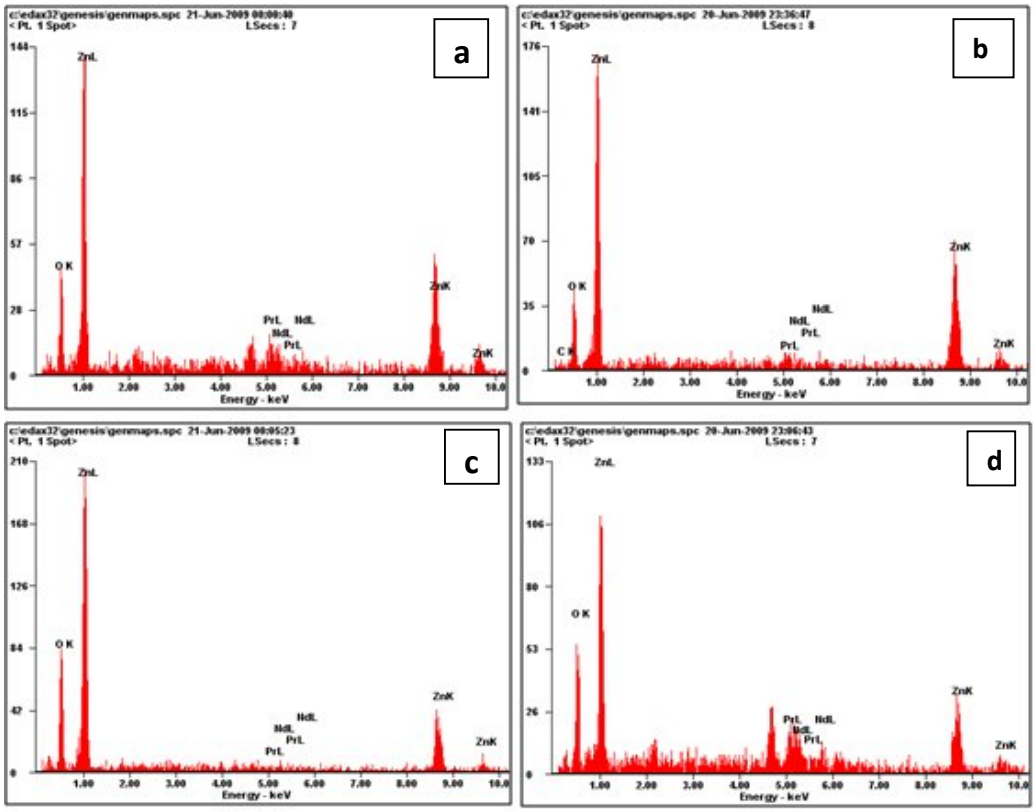

Fig (3.16): EDX spectra of the Di doped ZnO (a) 0.5% Di, (b) 1% Di, (c) 3% Di, (d) 5% Di

Table 3.3: List of elements present in samples, doped with different concentration of Di

Element	**0.5% Di**		**1% Di**		**3%Di**		**5%Di**	
	Wt%	At%	Wt%	At%	Wt%	At%	Wt%	At%
OK	-	-	11.85	17.07	29.36	64.01	17.83	54.53
PrL	-	-	06.15	31.78	02.17	00.54	19.58	06.80
NdL	-	-	03.95	01.87	03.71	00.90	19.97	06.77
Znk	-	-	73.27	48.09	64.76	34.56	42.62	31.90

The EDX spectra of the Di doped samples is shown in figure 3.16. The concentration of the different element observed, was listed in the table 3.1. We observed that the all the

samples are rich with Zinc and Oxygen element along with the small amount of Nd and Pr. The percentage of the Nd (Neodymium) and Pr (Praseodymium) increase at higher concentration due to the residue of unreacted part of Di at these concentrations.

➢ Chemical analysis of didymium doped ZnO:

- **FTIR spectra of Di doped ZnO Calcined at 400^0C**

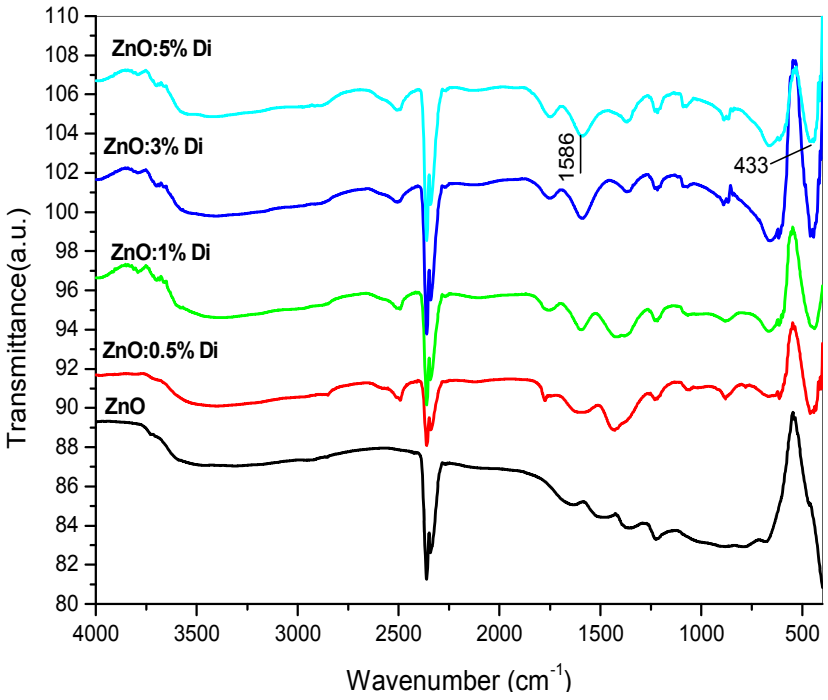

Fig(3.17): Comparison of didymium doped ZnO at different concentration after calcination at 400^oC

FTIR spectra of Di doped sample at concentration 0.5%, 1%, 3%, 5% is shown in figure 3.17 respectively. No significant change was observed in these samples as compared to the pure synthesized ZnO.

3.3.2 Effect of silver doping on ZnO:

➢ Structural and morphological analysis of Silver doped ZnO:

XRD analysis:

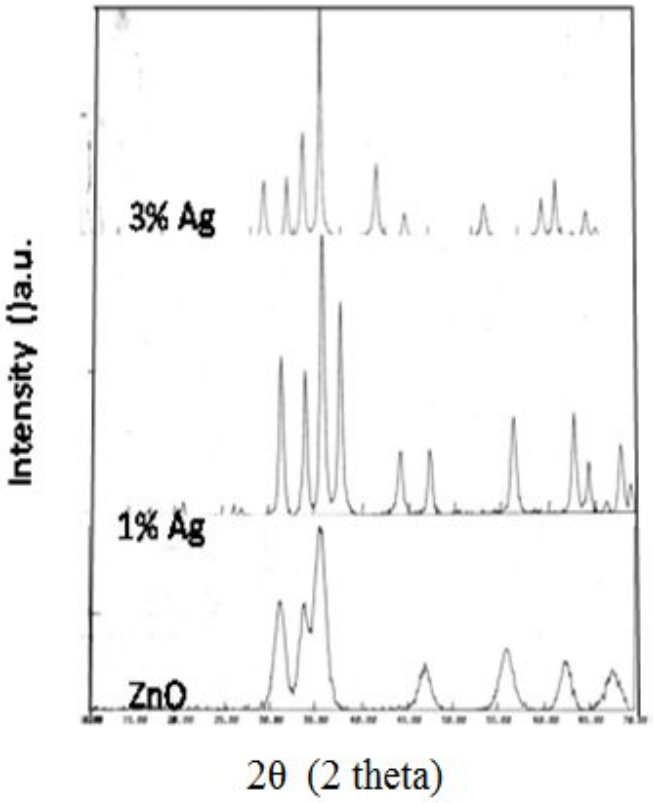

Fig (3.18): XRD patterns of Ag doped ZnO at different concentration

Figure 3.18 shows the XRD pattern of the Ag doped ZnO .We observed that the samples were polycrystalline in nature as the fine peaks with higher intensity were extended over 2θ scale. Some peaks observed in the sample was matched with JCPDS card no. 50664 (ZnO) however, the peaks at $2\theta = 36.8^0$, 44.1^0, 64.3^0 matched with JCPDS card no. 40783. From the XRD pattern we conclude the synthesized materials forming the mixed phase and the Ag ions is not going to the valance site of Zn.

SEM images of Ag doped ZnO:

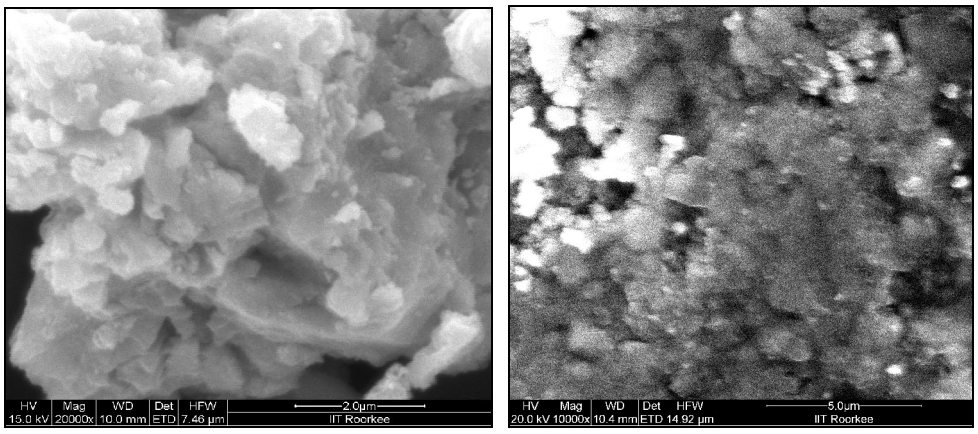

(a) **(b)**

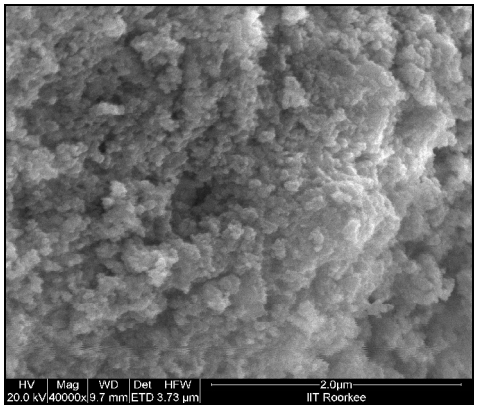

(c)

Fig (3.19): SEM image of (a) ZnO at 20,000X, (b) 1% Ag doped ZnO at 10,000X, (c) 3% Ag doped ZnO at 40,000X

SEM images of Ag doped sample are shown in the figure 3.19. We observed that the material is not forming any definite morphology, cluster of small grains was observed.

➢ Chemical analysis of Ag doped ZnO:

FTIR Spectra of Ag doped ZnO

FTIR spectrum of the Ag doped ZnO sample calcined at 400^0C for 1 hour shown in figure 3.20.

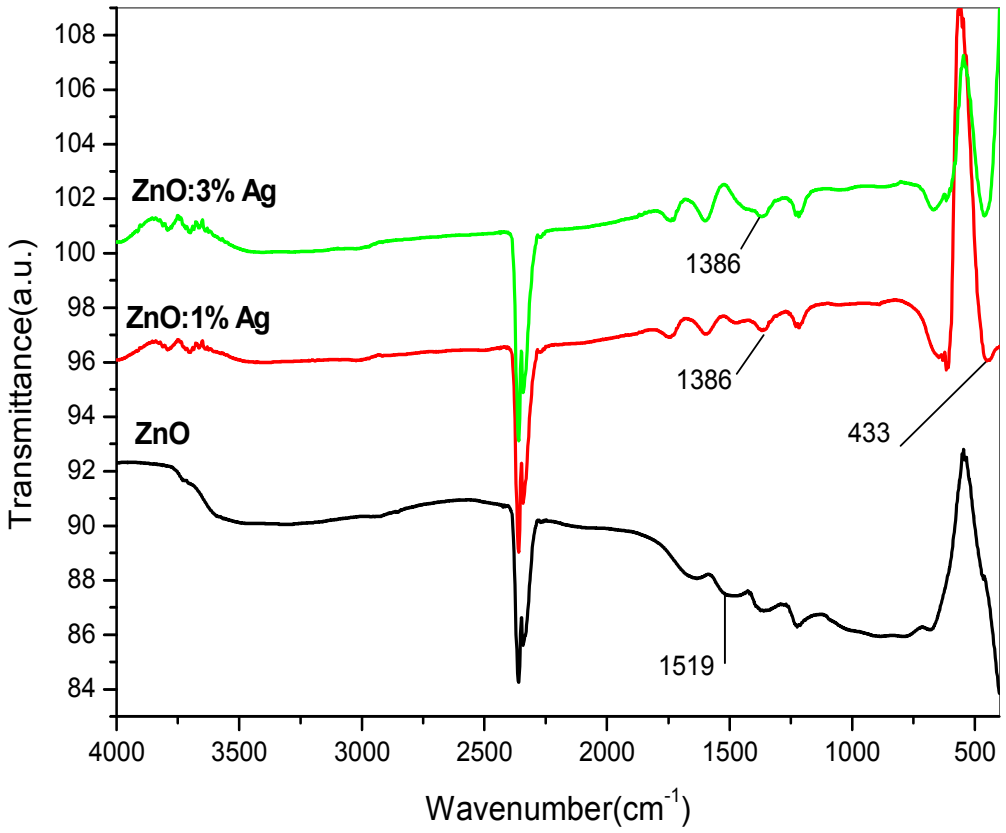

Figure 3.20: FTIR spectrum of the Ag doped ZnO in different concentration at 400^0 C

Peaks observed at 1519 cm^{-1} and 433 cm^{-1} corresponds to the COO^- group and Zn-O stretching respectively. Peak located at 1386 (cm^{-1}) gives the information about the presence of N-O group which may be due to the presence of nitrate group of $AgNO_3$.

Conclusion:

- We have successfully synthesized the single phase ZnO by using Sol gel method in basic medium having particle size about 4.8 nm. The synthesized system is also having band gap of 3.24 eV which is comparable with the standard value.

- Sample prepared by surfactant mediated growth also showing good crystallinity and pure single phase of ZnO having wurtzite hexagonal structure. However exact role of the surfactant is not visualised from the SEM images because of the limitation of SEM instrument up to micro range. Further to analyse the role of surfactant and morphology of particles we need to characterize these samples with TEM.

- We also studied the effect of calcination (at 400^0C for 1 hour) on these samples. We observed that calcination improve the crystallinity of the sample, due to the evaporation of lower melting point additive which bound the ZnO compound in as synthesized samples.

- We successfully dope the ZnO with Di ion up to 1% concentration .The XRD pattern shows the formation of pure phase of ZnO having wurtzite hexagonal structure. But at higher concentration of Di (3%, 5%) the system shows mixed phase as evident from the XRD analysis.

- Finally we also made an attempt to dope the Ag on the valance site of ZnO. But we fail to achieve the pure phase of ZnO. As reflected from XRD analysis that the Ag is showing its own peaks along with the ZnO peaks.

References:

[1] W. L. Hughes "Synthesis and characterization of ZnO for piezoelectric applications", PhD thesis, School of materials science & engineering, Georgia institute of technology USA. (2006)

[2] Ü. Özgür, Ya. I. Alivov, C. Liu, A. Teke, M. A. Reshchikov, S. Dogan, V. Avrutin, S.J. Cho and H. Morkoçd, journal of applied physics 98,041301(2005)

[3] Chumming Jin "Growth and characterization of ZnO and ZnO-based Alloys- $Mg_xZn_{1-x}O$ and $Mn_xZn_{1-x}O$" PhD thesis, Department of materials science and Engineering, North Carolina state university, Raleigh. (2003)

[4] G.Ferblantier, F. Mailly, R. Al Asmar, A. Foucaran, F. Pascal-Delannoy sensor and actuators A 122 184-188 (2005)

[5] Wolfgang H.Hirchwald Acc.Res., 18,228-234(1985)

[6] R. L. Hoffman, B. J. Norris and J. F. Wager, volume 82, Number 5 (2002)

[7] H. S. Bae and Seongil Im, applied physics letter 12, 123-127 (2003)

[8] Luis Manuel Angelats "Silva Study of structural, electrical, optical and magnetic properties of ZnO based films produced by magnetron sputtering" PhD thesis, university of Puerto Rico UPR. (2006)

[9] S.J. Pearton, D.P. Norton, K. Ip, Y.W. Heo, T. Steinerb, Superlattices and Microstructures 34 29–32 (2003)

[10] Günter Horst "The characterization of bulk as-grown and annealed ZnO by Hall effect" PhD thesis, University of Pretoria, Pretoria.

[11] W. Göpel, J. Pollmann, I. Ivanov and B. Reihl, Phys. Rev. B 26 (1982) 3144-3150.

[12] N. Izyumskaya, V. Avrutin, Ü. Özgür, Y. I. Alivov, and H. Morkoç phys. stat. sol. 244, No. 5, 1439–1450 (2007)

[13] Y. Ryu, Tae-Seok. Lee, J. A. Lubguban, H. W. White, Bong-Jin Kim, Yoon-Soo Park, and Chang-Joo Youn, Appl. Phys. Lett. 88, 241108 (2006).

[14] L. Stolt, J. Hedstrom, M. Ruckh, K.V. Velthaus, and H. W. Schcok, Appl. Phys. Letter, 62, 597, (1993).

[15] S. Shionoya, W.M. Yen, Phosphor Hood book, CRC Press, Boca Raton, FL, (1999), p255.

[16] R. R. Reeber, J. Appl. Phys. 41, 5063 (1970)

[17] T. Olorunyolemi, A. Birnboim, Y. Carmel, O. C. Wilson, Jr., and I. K. Lloyd, J. Am. Ceram. Soc. 85, 1249 (2002).

[18] D. I. Florescu, L. G. Mourokh, F. H. Pollak, D. C. Look, G. Cantwell, X. Li, J. Appl. Phys. 91, 890 (2002).

[19] D. C. Look, J. W. Hemsky, J. R. Sizelove, Phys. Rev. letters Vol. 82, No. 12 (1999).

[20] Chennupati Jagadish and Stephen J.Pearton "Zinc Oxide Bulk, Thin films and edition (2006).

[21] C. H. Park, S. B. Zhang, and S.-H. Wei, Phys. Rev. B 66, 073202 (2002).

[22] S. Tu¨zemen, Emre Gu¨ r, Optical Materials 30, 292–310 (2007).

[23] C. W. Bunn, "The lattice-dimensions of zinc oxide," Proc. Phys. Soc. London 47: 835, (1935).

[24] D. R. Lide (editor), CRC Handbook of Chemistry and Physics, CRC Press, New York, 73 edition, (1992).

[25] D. C. Look, "Recent advances in ZnO materials and devices," Mat. Sci. Eng. B. 80: 383, (2001).

[26] D. C. Look, D. C. Reynolds, J. R. Sizelove, R. L. Jones, C. W. Litton, G. Cantwell and W. C. Harsch, "Electrical properties of bulk ZnO," Solid State Commun. 105: 399, (1998).

[27] Y. Segawa, A. Ohtomo, M. Kawasaki, H. Koinuma, Z. K. Tang, P. Yu and G. K. L. Wong, "Growth of ZnO thin films by laser-MBE: Lasing of excitons at room temperature," Phys. Stat. Sol. 202: 669, (1997).

[28] J. E. Nause, "ZnO broadens the spectrum," III-Vs Review 12: 28, 1999. 7. J. E. Nause, "Fluorescent substrate offers route to phosphor-free LEDs," Comp. Semicond. 11: 29, (2005).

[29] S. O. Kucheyev, J. S. Williams, C. Jagadish, J. Zou, C. Evans, A. J. Nelson and A. V.Hamza, "Ion- beam-produced structural defects in ZnO," Phys. Rev. B 67: 094 115, (2003).

[30] C. Coskun, D. C. Look, G. C. Farlow and J. R. Sizelove, "Radiation hardness of ZnO at low temperatures," Semicond. Sci. Technol. 19: 752, (2004).

[31] S. O. Kucheyev, J. S. Williams and C. Jagadish, "Ion-beam-defect processes in group-III nitrides and ZnO," Vacuum 73: 93, (2004).

[32] N. A. Spaldin, "Search for Ferromagenetism in transition-metal-doped piezoelectric ZnO," Phys. Rev. B 69: 125 201, (2004).

[33] S. J. Pearton, D. P. Norton, K. Ip, Y. Heo and T. Steiner, "Recent advances in processing of ZnO," J. Vac. Sci. Technol. B 22: 932, (2004).

[34] D. C. Look and B. Claflin, "P-type doping and devices based on ZnO," Phys. Stat. Sol. (b) 241: 624, (2004).

[35] D. C. Look, B. Claflin, Y. I. Alivov and S. J. Park, "The future of ZnO light emitters," Phys. Stat. Sol. (a) 201: 2203, (2004).

[36] S. B. Zhang, S. H. Wei and A. Zunger, "Intrinsic n-type versus p-type doping asymmetry and the defect physics of ZnO," Phys. Rev. B 63: 075 205, (2001).

[37] A. F. Kohan, G. Ceder, D. Morgan and C. G. Van deWalle, "First-principles study of native point defects in ZnO," Phys. Rev. B 61: 15 019, (2000).

[38] C. G. Van de Walle, "Hydrogen as a cause of doping in ZnO," Phys. Rev. Lett. 85: 1012, (2000).